



# Ensemble-based satellite-derived carbon dioxide and methane column-averaged dry-air mole fraction data sets (2003-2018) for carbon and climate applications

5 Maximilian Reuter<sup>1</sup>, Michael Buchwitz<sup>1</sup>, Oliver Schneising<sup>1</sup>, Stefan Noël<sup>1</sup>, Heinrich Bovensmann<sup>1</sup>,  
John P. Burrows<sup>1</sup>, Hartmut Boesch<sup>2,3</sup>, Antonio Di Noia<sup>2,3</sup>, Jasdeep Anand<sup>2,3</sup>, Robert J. Parker<sup>2,3</sup>, Peter  
Somkuti<sup>2,3,8</sup>, Lianghai Wu<sup>4</sup>, Otto P. Hasekamp<sup>4</sup>, Ilse Aben<sup>4</sup>, Akihiko Kuze<sup>5</sup>, Hiroshi Suto<sup>5</sup>, Kei Shiomi<sup>5</sup>,  
Yukio Yoshida<sup>6</sup>, Isamu Morino<sup>6</sup>, David Crisp<sup>7</sup>, Christopher W. O'Dell<sup>8</sup>, Justus Notholt<sup>1</sup>, Christof Petri<sup>1</sup>,  
10 Thorsten Warneke<sup>1</sup>, Voltaire A. Velazco<sup>9</sup>, Nicholas M. Deutscher<sup>9</sup>, David W. T. Griffith<sup>9</sup>, Rigel Kivi<sup>10</sup>,  
Dave Pollard<sup>11</sup>, Frank Hase<sup>12</sup>, Ralf Sussmann<sup>13</sup>, Yao V. Té<sup>14</sup>, Kimberly Strong<sup>15</sup>, Sébastien Roche<sup>15</sup>,  
Mahesh K. Sha<sup>16</sup>, Martine De Mazière<sup>16</sup>, Dietrich G. Feist<sup>17,18,19</sup>, Laura, T. Iraci<sup>20</sup>, Coleen M. Roehl<sup>21</sup>,  
Christian Retscher<sup>22</sup>, Dinand Schepers<sup>23</sup>

<sup>1</sup>Institute of Environmental Physics (IUP), University of Bremen, 28334 Bremen, Germany

15 <sup>2</sup>Earth Observation Science, University of Leicester, LE1 7RH, Leicester, UK

<sup>3</sup>NERC National Centre for Earth Observation, LE1 7RH, Leicester, UK

<sup>4</sup>SRON Netherlands Institute for Space Research, 3584 CA Utrecht, The Netherlands

<sup>5</sup>Japan Aerospace Exploration Agency (JAXA), 305-8505, Tsukuba, Japan

<sup>6</sup>National Institute for Environmental Studies (NIES), 305-8506, Tsukuba, Japan

20 <sup>7</sup>Jet Propulsion Laboratory (JPL), Pasadena, CA 91109, USA

<sup>8</sup>Cooperative Institute for Research in the Atmosphere, Colorado State University (CSU), Fort Collins, CO 80523, USA

<sup>9</sup>Centre for Atmospheric Chemistry, School of Earth, Atmospheric and Life Sciences, University of Wollongong, NSW,  
2522, Australia

<sup>10</sup>Finnish Meteorological Institute (FMI), 99600 Sodankylä, Finland

25 <sup>11</sup>National Institute of Water and Atmospheric Research (NIWA), Lauder, New Zealand

<sup>12</sup>Karlsruhe Institute of Technology (KIT), Institute of Meteorology and Climate Research (IMK), IMK-ASF, 76021  
Karlsruhe, Germany

<sup>13</sup>Karlsruhe Institute of Technology (KIT), Institute of Meteorology and Climate Research (IMK), IMK-IFU, 82467  
Garmisch-Partenkirchen, Germany



- 30 <sup>14</sup>Laboratoire d'Etudes du Rayonnement et de la Matière en Astrophysique (LERMA-IPSL), Sorbonne Université, CNRS,  
Observatoire de Paris, PSL Université, 75005 Paris, France
- <sup>15</sup>Department of Physics, University of Toronto, Toronto, ON, M5S 1A7, Canada
- <sup>16</sup>Royal Belgian Institute for Space Aeronomy (BIRA-IASB), 1180 Uccle, Belgium
- <sup>17</sup>Max Planck Institute for Biogeochemistry, 07745 Jena, Germany
- 35 <sup>18</sup>Lehrstuhl für Physik der Atmosphäre, Ludwig-Maximilians-Universität München, 80333 München, Germany
- <sup>19</sup>Institut für Physik der Atmosphäre, Deutsches Zentrum für Luft- und Raumfahrt Oberpfaffenhofen, 82234 Weßling,  
Germany
- <sup>20</sup>Atmospheric Science Branch, National Aeronautics and Space Administration (NASA), Moffett Field, CA 94035, USA
- <sup>21</sup>California Institute of Technology, Pasadena, CA 91125, USA
- 40 <sup>22</sup>European Space Agency (ESA), ESRIN, 00044 Frascati, Italy
- <sup>23</sup>European Centre for Medium-Range Weather Forecasts (ECMWF), Reading RG2 9AX, UK

*Correspondence to:* Michael Buchwitz (buchwitz@uni-bremen.de)

**Abstract.** Satellite retrievals of column-averaged dry-air mole fractions of carbon dioxide (CO<sub>2</sub>) and methane (CH<sub>4</sub>),  
45 denoted XCO<sub>2</sub> and XCH<sub>4</sub>, respectively, have been used in recent years to obtain information on natural and anthropogenic  
sources and sinks and for other applications such as comparisons with climate models. Here we present new data sets based  
on merging several individual satellite data products in order to generate consistent long-term Climate Data Records (CDRs)  
of these two Essential Climate Variables (ECVs). These ECV CDRs, which cover the time period 2003-2018, have been  
generated using an ensemble of data products from the satellite sensors SCIAMACHY/ENVISAT, TANSO-FTS/GOSAT  
50 and (for XCO<sub>2</sub>) for the first time also including data from the Orbiting Carbon Observatory-2 (OCO-2) satellite. Two types  
of products have been generated: (i) Level 2 (L2) products generated with the latest version of the “ensemble median  
algorithm” (EMMA) and (ii) Level 3 (L3) products obtained by gridding the corresponding L2 EMMA products to obtain a  
monthly 5°x5° data product in Obs4MIPs (Observations for Model Intercomparisons Project) format. The L2 products  
consists of daily NetCDF (Network Common Data Form) files, which contain in addition to the main parameters, i.e., XCO<sub>2</sub>  
55 or XCH<sub>4</sub>, corresponding uncertainty estimates for random and potential systematic uncertainties and the averaging kernel for  
each single (quality-filtered) satellite observation. We describe the algorithms used to generate these data products and  
present quality assessment results based on comparisons with Total Carbon Column Observing Network (TCCON) ground-  
based retrievals. We found that the XCO<sub>2</sub> Level 2 data set at the TCCON validation sites can be characterized by the  
following figures of merit (the corresponding values for the Level 3 product are listed in brackets): single observation  
60 random error (1-sigma): 1.29 ppm (monthly: 1.18 ppm); global bias: 0.20 ppm (0.18 ppm), spatio-temporal bias or “relative  
accuracy” (1-sigma): 0.66 ppm (0.70 ppm). The corresponding values for the XCH<sub>4</sub> products are: single observation random  
error (1-sigma): 17.4 ppb (monthly: 8.7 ppb); global bias: -2.0 ppb (-2.9 ppb), spatio-temporal bias (1-sigma): 5.0 ppb (4.9



ppb). It has also been found that the data products exhibit very good long-term stability as no significant long-term bias trend has been identified. The new data sets have also been used to derive annual XCO<sub>2</sub> and XCH<sub>4</sub> growth rates, which are in reasonable to good agreement with growth rates from the National Oceanic and Atmospheric Administration (NOAA) based on marine surface observations. The presented ECV data sets are available (from December 2019 onwards) via the Climate Data Store (CDS, <https://cds.climate.copernicus.eu/>) of the Copernicus Climate Change Service (C3S, <https://climate.copernicus.eu/>).

## 70 1 Introduction

Carbon dioxide (CO<sub>2</sub>) and methane (CH<sub>4</sub>) are important greenhouse gases and increasing atmospheric concentrations result in global warming with adverse consequences such as sea level rise (IPCC, 2013). Because of their importance for climate, these gases have been classified as Essential Climate Variables (ECVs) by the Global Climate Observing System (GCOS) (GCOS-154, 2010; GCOS-200, 2016). The generation of XCO<sub>2</sub> and XCH<sub>4</sub> satellite-derived ECV data products meeting GCOS requirements using European satellite retrieval algorithms started in 2010 in the framework of the GHG-CCI project (<http://www.esa-ghg-cci.org/>) of the European Space Agency's (ESA) Climate Change Initiative (CCI) (Hollmann et al., 2013). Since the end of 2016, this activity continues operationally via the Copernicus Climate Change Service (C3S, <https://climate.copernicus.eu/>) and the corresponding CO<sub>2</sub> and CH<sub>4</sub> data products are available via the Copernicus Climate Data Store (CDS, <https://cds.climate.copernicus.eu/>). These ECV data products have been used for a range of applications such as improving our knowledge of CO<sub>2</sub> and/or CH<sub>4</sub> surface fluxes (e.g., Alexe et al., 2015; Basu et al., 2013; Buchwitz et al., 2017a; Chevallier et al., 2014, 2015; Ganesan et al., 2017; Gaubert et al., 2019; Houweling et al., 2015; Liu et al., 2017; Maasackers et al., 2019; Miller et al., 2019; Reuter et al., 2014a, 2014b, 2019a; Sheng et al., 2018; Schneising et al., 2014b; Turner et al., 2015, 2019), comparison with climate and other models (e.g., Hayman et al., 2014; Lauer et al., 2017; Schneising et al., 2014a) and for other applications such as computation of CO<sub>2</sub> growth rates (e.g., Buchwitz et al., 2018) and to better understand changes of the amplitude of the CO<sub>2</sub> seasonal cycle (e.g., Yin et al., 2018).

The C3S satellite greenhouse gas (GHG) data set consists of single-sensor satellite data products and of merged (i.e., combined multi-sensor, multi-algorithm) data products. Here we present the latest version, version 4.1, of the merged Level 2 (L2) and merged Level 3 (L3) XCO<sub>2</sub> and XCH<sub>4</sub> data products, which cover the time period 2003-2018. The L2 products (XCO<sub>2</sub>\_EMMA and XCH<sub>4</sub>\_EMMA) have been compiled with the ensemble median algorithm EMMA originally proposed by Reuter et al., 2013, and recent modifications, which are described in Sect. 3.1. These products contain detailed information for each single observation (i.e., footprint or ground pixel) including time, latitude and longitude, the main parameter (i.e., XCO<sub>2</sub> or XCH<sub>4</sub>), its stochastic uncertainty (e.g., due to instrument noise), an estimate of potential systematic uncertainties (e.g., due to spatial or temporal bias patterns), its averaging kernel and corresponding *a priori* profile. The L3 products (XCO<sub>2</sub>\_OBS4MIPS and XCH<sub>4</sub>\_OBS4MIPS) are gridded products at monthly time and 5°x5° spatial resolution in Obs4MIPs (Observations for Model Intercomparisons Project, <https://www.earthsystemcog.org/projects/obs4mips/>) format.



Figure 1 provides an overview of the resulting merged XCO<sub>2</sub> data product in terms of time series for three latitude bands and global maps and the similarly structured Fig. 2 shows the XCH<sub>4</sub> product. As can be seen, XCO<sub>2</sub> and XCH<sub>4</sub> are both increasing with time and exhibit seasonal fluctuations and spatial variations. The spatio-temporal characteristics of the data, e.g., the spatial sampling, reflects the characteristics of the underlying individual sensor satellite data (described in the data section, Sect. 2). Figure 1 and 2 are discussed in detail in the results section, Sect. 4. How these data products have been generated is described in the methods section, Sect. 3. A summary and conclusions are given in Sect. 5.

## 2 Data

In this section, we present an overview about the input data used to generate and validate the new XCO<sub>2</sub> and XCH<sub>4</sub> data products.

### 2.1 Satellite data

The input satellite data used to generate the merged satellite data products are individual satellite sensor Level 2 (L2) data products. Table 1 provides an overview about the satellite XCO<sub>2</sub> input data sets. As can be seen, in total 8 XCO<sub>2</sub> L2 data products have been used to generate the merged L2 and Level 3 (L3) XCO<sub>2</sub> data products, each corresponding to a different combination of satellite sensor and retrieval algorithm. An overview about the time coverage of these input data products is presented in Fig. 3. As can be seen, the time period 2003 to March 2009 is only covered by one XCO<sub>2</sub> product, namely XCO<sub>2</sub> retrieved with the Bremen optimal ESTimation DOAS (BESD) algorithm (Reuter et al., 2010, 2011) from the SCIAMACHY/ENVISAT (Bovensmann et al., 1999) instrument. A second SCIAMACHY XCO<sub>2</sub> data product is available, which has been retrieved with the Weighting-Function-Modified-Differential-Optical-Absorption-Spectroscopy (WFM-DOAS or WFMD) algorithm (Schneising et al., 2011), but this product is not used because the merging algorithm EMMA (Ensemble Median Algorithm, Reuter et al., 2013, described in Sect. 3.1) requires one or more than two input data products. Therefore, one of the two products had to be selected and the choice was the BESD product for XCO<sub>2</sub> because of somewhat higher data quality compared to the WFMD product (Buchwitz et al., 2017b) (note however that the WFMD product has the advantage of containing a larger number of observations). As can be seen from Tab. 1 and Fig. 3, several GOSAT input products have been used from April 2009 onwards and two OCO-2 XCO<sub>2</sub> products from 09/2014 and 01/2015 onwards. Note that additional algorithms / data products are available but have not been used as input, for example the GOSAT BESD XCO<sub>2</sub> product (Heymann et al., 2015) and the OCO-2 RemoTeC XCO<sub>2</sub> product (Wu et al., 2018). These or other additional products may be added in future versions of the merged XCO<sub>2</sub> products.

All listed satellites perform nadir (down-looking) and glint observations and provide radiance spectra covering the relevant CO<sub>2</sub> and CH<sub>4</sub> absorption bands located in the short-wave infrared (SWIR) part of the electromagnetic spectrum (around 1.6 μm and 2 μm) and also cover the O<sub>2</sub> A-band spectral region in the near-infrared (NIR, around 0.76 μm). All individual sensor input L2 data products have been generated using retrieval algorithms based on minimizing the difference of a



modelled radiance spectrum to the observed spectrum by modifying so called state vector elements (for details we refer to the references listed in Tab. 1; for additional information see also the Algorithm Theoretical Basis Documents (ATBDs) Buchwitz et al., 2019b, and Reuter et al., 2019b). The exact definition of the state vector depends on the algorithm but the general approach is based on the “Optimal Estimation” (Rodgers, 2000) formalism or similar approaches (see references Tab. 1). Among the state vector elements is a representation of the CO<sub>2</sub> vertical profile but also other parameters to consider interfering gases (e.g., water vapour), surface reflection, atmospheric scattering and other effects and parameters, which have an impact on the (interpretation of the) measured radiance spectrum.

Table 2 and Fig. 4 provide an overview about the satellite XCH<sub>4</sub> L2 input data sets. As for XCO<sub>2</sub>, the time period 2003 to March 2009 is only covered by one SCIAMACHY data product. From April 2009 onwards several GOSAT XCH<sub>4</sub> products are available (see Tab. 2) and have been used to generate the merged XCH<sub>4</sub> data L2 and L3 data products. For future updates it is also planned to include XCH<sub>4</sub> from the Sentinel-5 Precursor (S5P) satellite (Veefkind et al., 2012) but S5P XCH<sub>4</sub> (Hu et al., 2018; Schneising et al., 2019) has not yet been included as the time period covered by these products is currently is still quite short (less than 2 years) but it will be aimed at to include S5P XCH<sub>4</sub> for one of the next updates of the merged methane products.

## 2.2 Ground-based data

The satellite data products have been validated by comparison with the XCO<sub>2</sub> and XCH<sub>4</sub> data products of the Total Carbon Column Observing Network (TCCON, Wunch et al., 2011). TCCON is a network of ground-based Fourier Transform Spectrometers (FTS) recording direct solar spectra in the NIR/SWIR spectral region. From these spectra, accurate and precise column-averaged abundances of CO<sub>2</sub>, CH<sub>4</sub> and a number of other species are retrieved. The TCCON data products (version GGG2014) have been obtained via the TCCON data archive (<https://tccodata.org/>, last access 15-July-2019). An overview about the used TCCON sites is presented in Tab. 3.

In Sect. 4.3, we present annual XCO<sub>2</sub> and XCH<sub>4</sub> growth rates, which have been derived from the new XCO<sub>2</sub> and XCH<sub>4</sub> OBS4MIPS data products using the method described in Buchwitz et al., 2018. These growth rates are compared with growth rates derived from marine surface CO<sub>2</sub> and CH<sub>4</sub> observations, which have been obtained from the National Oceanic and Atmospheric Administration (NOAA) (for details including links and last access see section Acknowledgements).

## 3. Methods

### 3.1 Merging algorithm EMMA

In order to generate the merged L2 products, the Ensemble Median Algorithm (EMMA) is used, which is described in detail in Reuter et al., 2013. Therefore, we limit the description given here to a short overview of the latest version of the EMMA



160 algorithm. To be specific, we initially describe the EMMA XCO<sub>2</sub> algorithm and explain differences relevant for XCH<sub>4</sub> at the end of this sub-section.

The EMMA XCO<sub>2</sub> data product consists of selected individual L2 soundings from the available individual sensor L2 input products (listed in Tab. 1). The EMMA L2 product is based on selecting “the best” soundings (i.e., single ground pixel observations) from the ensemble of individual sensor L2 products. Sounding selection is based on monthly time and 10°x10°  
165 spatial intervals. To decide which individual product is selected for a given month and given grid cell, all input products are first gridded (monthly, 10°x10°) to consider the fact that the spatio-temporal sampling is different for each individual product (due to different satellite sensors and algorithm dependent quality filtering strategies). The selected product is the median in terms of average XCO<sub>2</sub> per month and grid cell (note that in case of an even number of products the product which is closest to the mean is selected). The median is used primarily to remove potential outliers. The advantage of the median is also (in  
170 contrast to, for example, the arithmetic mean) that no averaging or other modifications to the input data are required. In order for a grid cell to be assigned a valid value, the following criterion has to be fulfilled: a minimum number of data products has to be available (see grey area in Fig. 3) having a standard error of the mean (SEOM) of less than 1 ppm. SEOM is defined by  $\frac{1}{n}\sqrt{\sum_i \sigma_i^2}$ , with  $\sigma_i$  being the (scaled, see below) XCO<sub>2</sub> uncertainty of the *i*-th out of *n* soundings.

This means that EMMA selects for each month and each 10°x10° grid cell exactly one product of the available individual L2  
175 input products and then “transfers” all relevant information (i.e., XCO<sub>2</sub> and its uncertainty, related averaging kernels and *a priori* profile, etc.) from the selected original L2 file into the corresponding daily EMMA L2 product file. This ensures that most of the original information from the selected individual product is also contained in the merged product.

However, some modifications are applied. In order to remove (or at least to minimize) the impact of different *a priori* assumptions, all products are converted to common *a priori* CO<sub>2</sub> vertical profiles (see Reuter et al., 2013, for details). The  
180 new *a priori* profiles are obtained from the Simple Empirical CO<sub>2</sub> Model (SECM, Reuter et al., 2012). SECM is essentially an empirically found function with parameters optimized using a CO<sub>2</sub> model (CT2017, see below). The SECM model used here is referred to as SECM2018 and is an update of the SECM model described in Reuter et al., 2012. The main difference is that SECM2018 is using a recent version of NOAA’s assimilation system CarbonTracker (Peters et al., 2007, with updates documented at <http://carbontracker.noaa.gov/>), namely CT2017.

185 SECM2018 is also used to correct for potential offsets between the individual data products by adding or subtracting a global offset (i.e., by using one constant offset value for each individual product applied globally and for the full time series). Time series of the individual data products before and after offset correction are shown in Fig. 5. Note that in Fig. 5 all data are relative to SECM2018, which is a very simple CO<sub>2</sub> model and therefore all variations and trends seen in Fig. 5 are at least to some extent model errors. As can be seen from Fig. 5, the correction brings the individual data sets typically closer together  
190 without changing any of their other characteristics (e.g., their time dependence). But as can also be seen from Fig. 5, “better agreement” is only achieved “on average”, not necessarily for all products during the entire time period. For example, the





GOSAT RemoTeC product (blue curve) during 2009-2012 exhibits a somewhat larger difference after the offset correction. The approx. 2 ppm (0.5%) spike at the beginning of the time series is likely due to a positive bias of the underlying BESD data product, which has not been corrected due to lack of reference data in this time period (see also the discussion of this aspect in Buchwitz et al., 2018). An obvious issue is also the approximately 1.5 ppm (0.4%) discontinuity in the first half of 2014 of the PPDF-S product (light green curve). Depending on application, this may be an issue when this product is used stand-alone but this is not a problem for EMMA as EMMA identifies and ignores outliers.

Another modification applied to the individual L2 input products is a potential scaling of their reported uncertainty for the individual L2 soundings. The scaling factor has been chosen such that on average the uncertainty of the reported error is consistent with the standard deviation of satellite minus ground-based validation data differences (see Sects. 4.1 for the validation of the reported uncertainties via the “Uncertainty ratio”).

In order to avoid that an individual input product, which has much more observations than the other products (such as OCO-2 compared to GOSAT), entirely dominates the EMMA product, a method has been implemented to prevent over-weighting the contributions from individual L2 input data products. The method is based on limiting the number of data points (per grid cell and month) chosen from this algorithm. This is done by computing SEOM for each month, grid cell, and algorithm. For each grid cell and month we then compute a SEOM threshold by the 25<sup>th</sup> percentile of SEOMs divided by  $\sqrt{2}$ . If SEOM of an algorithm is smaller than the computed threshold, a subset of soundings is randomly chosen such that SEOM becomes just larger than the threshold. If, for example all  $\sigma_i$  are 1 ppm, then SEOM simply becomes  $1/\sqrt{n}$ . If in this case, for example, data from 4 algorithms are available with  $n_1 = 60$ ,  $n_2 = 80$ ,  $n_3 = 100$ , and  $n_4 = 1000$ , the SEOM threshold would become  $1/\sqrt{2 n_3}$ , which would effectively limit the number of soundings of the fourth algorithm to 200 (chosen randomly).

In addition to the L2 information of the selected data products, EMMA stores the following diagnostic information for each selected sounding: identifier for the selected L2 algorithm and inter-algorithm spread (IAS) within the grid box of the sounding. Within each grid box, IAS is defined as the algorithm-to-algorithm standard deviation of the grid box averages.

The EMMA L2 XCH<sub>4</sub> product has been generated similarly as the EMMA L2 XCO<sub>2</sub> product, i.e., using essentially the same method as described above. A difference is that the offset correction has been done with a CH<sub>4</sub> model instead of SECM2018. This model is the “Simple CH<sub>4</sub> Climatological model” (SC4C) and we use the year 2018 update referred to as SC4C2018 in the following. The SC4C2018 model is similar as SECM2018 but for XCH<sub>4</sub>. It is a model-based CH<sub>4</sub> climatology adjusted for the annual growth rate (note that this model has also been used as climatological training and calibration data set as described in Schneising et al., 2019). The EMMA algorithm SEOM limit controlling the minimum number of data points per grid box, month, and algorithm has been set to 12 ppb for XCH<sub>4</sub>. The impact of the offset correction for merging the XCH<sub>4</sub> products is shown in Fig. 6. Note that in Fig. 6 all data are relative to SC4C2018, which is a very simple CH<sub>4</sub> model and therefore all variations and trends seen in Fig. 6 are at least to some extent model errors. As for



CO<sub>2</sub> (Fig. 5) the offset correction typically brings the various XCH<sub>4</sub> products closer together but does not change any of their  
225 other characteristics. The PPDF-S product suffers from a discontinuity (of 8 ppb or 0.4%) in the first half of 2014 (see above  
for a similar problem for PPDF-S XCO<sub>2</sub>).

### 3.2 Algorithm to generate the Level 3 OBS4MIPS products

The version 4.1 L3 XCO<sub>2</sub>\_OBS4MIPS and XCH<sub>4</sub>\_OBS4MIPS data products have been obtained by gridding (averaging)  
230 the version 4.1 L2, i.e., XCO<sub>2</sub>\_EMMA and XCH<sub>4</sub>\_EMMA, products using monthly time and 5°x5° spatial resolution. The  
algorithm for the generation of the OBS4MIPS products is described in Reuter et al., 2019b. Therefore, we here provide only  
a short overview.

The gridding bases on arithmetic unweighted averaging of all soundings falling in a grid box. For each grid box, the standard  
error of the mean is computed using the uncertainties contained in the corresponding EMMA product files. In order to reduce  
235 noise at least two individual observations must be present and the resulting standard error of the mean must be less than 1.6  
ppm for XCO<sub>2</sub> and less than 12 ppb for XCH<sub>4</sub>.

Besides XCO<sub>2</sub> or XCH<sub>4</sub>, the final L3 product also includes (per grid box and month) the number of soundings used for  
averaging, the average column averaging kernel, the average *a priori* profile, the standard deviation of the averaged XCO<sub>2</sub> or  
XCH<sub>4</sub> values, and an estimate for the total uncertainty computed as root-sum-square of two values, where one value is  
240 SEOM and the other value is IAS as computed by EMMA. For cases including only one algorithm, the second value is  
replaced by quadratically adding spatial and seasonal accuracy determined from the TCCON validation.

### 3.3 Validation method

The validation of the merged satellite-derived XCO<sub>2</sub> and XCH<sub>4</sub> data products is based on comparisons with ground-based  
245 XCO<sub>2</sub> and XCH<sub>4</sub> TCCON observations (using version GGG2014). We present results from two somewhat different  
validation methods (the “EMMA method” (Reuter et al., 2013) and the “QA/QC method” (Buchwitz et al., 2017b), see  
below), which are similar to other validation methods used in recent years (e.g., Butz et al., 2010; Cogan et al., 2012; Dils et  
al., 2014; O’Dell et al., 2018; Parker et al., 2011). These methods differ with respect to details such as the chosen collocation  
criterion, whether the data are brought to a common *a priori* or not and if yes which *a priori* has been used. In the following,  
250 we will highlight some of these details as relevant for the two validation methods used for this manuscript.

Both methods used for the validation of the L2 EMMA products are based on collocating each individual satellite XCO<sub>2</sub> (or  
XCH<sub>4</sub>) observation with a corresponding value obtained from TCCON using pre-defined spatial and temporal collocation  
criteria (see below). The comparisons take into account different *a priori* assumptions regarding the vertical profiles of CO<sub>2</sub>  
(or CH<sub>4</sub>) as used for the generation of the L2 input products by converting either the satellite data (QA/QC method) or the





255 TCCON data (EMMA method) to a common *a priori*. This *a priori* correction is based on using the satellite averaging  
kernels and *a priori* profiles, which are contained (for each single observation) in the EMMA product files. The magnitude  
of the *a priori* correction (the explicit formula is shown as Eq. 3 in Dils et al., 2014) depends on the difference of the  
averaging kernel from unity and on the difference of the *a priori* profiles. Because the averaging kernel profiles are typically  
close to unity (note that both satellite and the TCCON retrievals correspond to cloud-free conditions) and because the *a*  
260 *a priori* profiles are not totally unrealistic, the *a priori* correction is typically very small (approximately 0.1 ppm for XCO<sub>2</sub> and  
1 ppb for XCH<sub>4</sub>).

The first validation method is the “EMMA quality assessment method”, which is described in Reuter et al., 2013. Note that  
EMMA is not only a “merging method” but also a “data quality assessment method”, as the assessment of the quality of all  
satellite input data (listed in Tabs. 1 and 2) is a key aspect of EMMA. The second method is the Quality Assessment /  
265 Quality Control (QA/QC) method (Buchwitz et al., 2017b), which is applied to all satellite XCO<sub>2</sub> and XCH<sub>4</sub> data products  
generated for the Copernicus Climate Change Service (C3S), i.e., to the merged products but also to all the individual sensor  
CCI/C3S L2 input products, which are also available via the Copernicus Climate Data Store (CDS) (see products with  
“CCI/C3S product ID” listed in Tabs. 1 and 2).

Key differences between the QA/QC method and the EMMA method are:

- 270 • Collocation criteria: QA/QC used  $\pm 2^\circ$  latitude and  $\pm 4^\circ$  longitude as spatial collocation criterion but EMMA used  
500 km (both methods use the same temporal collocation criterion of 2 hours).
- Filtering criterion surface elevation: EMMA requires a surface elevation difference of less than 250 m between a  
TCCON site and satellite footprints, whereas the QA/QC does not use this filtering criterion.
- *A priori* correction: both methods correct for the use of different *a priori* CO<sub>2</sub> vertical profiles in the various  
275 retrieval algorithms but QA/QC uses the TCCON *a priori* as common *a priori* whereas EMMA uses the  
SECM2018 model for CO<sub>2</sub> and the SC4C2018 model for CH<sub>4</sub> (see Sect. 3.1).
- Approach to quantify seasonal bias and linear bias trend: the EMMA method is based on fitting a trend model,  
which includes an offset-term, a slope-term and a sine-term for seasonal fluctuations (see Reuter et al., 2019c) and  
computes the seasonal bias from the standard deviation of the fitted seasonal fluctuation term and obtains the bias  
280 trend and its uncertainty from the fitted slope-term. The QA/QC method (Buchwitz et al., 2019a) uses (only) a  
linear fit to obtain the bias trend and its uncertainty and computes the seasonal bias from the standard deviation of  
the seasonal biases (as also done by Dils et al., 2014, for their quantity “seasonality”).
- Criteria for “enough data”: Both algorithms use several different thresholds for the required minimum number of  
collocations per TCCON site and minimum length of overlapping TCCON time series.

285 Despite all these differences, quite similar overall figures of merit have been obtained with both methods (see results section,  
Sect. 4). This indicates that the overall data quality results do not critically depend on the details of the assessment method



(the same conclusion has also been reported for earlier comparisons of results from different assessment methods (e.g., Buchwitz et al., 2015, 2017b)).

290

## 4. Results and discussion

### 4.1 Products XCO<sub>2</sub>\_EMMA and XCO<sub>2</sub>\_OBS4MIPS (v4.1)

When generating an EMMA product, a set of standard figures are generated such as Fig. 5 already discussed but also maps  
295 of the EMMA product and of the various input data products for all months of the 2003-2018 time period. Two of these  
figures are shown here, namely the figures for April 2011 (Fig. 7) and April 2015 (Fig. 8) (note that 2011 is the last full year  
with data from SCIAMACHY and that 2015 is the first full year with OCO-2 data). The maps in the first four rows of Figs. 7  
and 8 show the individual sensor/algorithm L2 input data. As can be seen, the spatial XCO<sub>2</sub> pattern are quite similar (e.g.,  
north-south gradient) but there are also significant differences, especially with respect to the spatial coverage. The spatial  
300 coverage depends on time and is related to the different satellite instruments but also due to algorithm dependent quality  
filtering. The largest differences are between the SCIAMACHY BESD product (top left in Fig. 7) compared to the other  
products, as the SCIAMACHY product is limited to observations over land, whereas the GOSAT and OCO-2 products also  
have some ocean coverage due to a special observation mode, namely the ocean-glint mode, which permits to get sufficient  
signal (and therefore also signal-to-noise) also over the ocean (note that the reflectivity of water is poor outside of sun-glint  
305 conditions in the used SWIR spectral regions around 1.6  $\mu\text{m}$  and 2  $\mu\text{m}$ ). The EMMA product is shown in the bottom left  
panels of Figs. 7 and 8 and in the bottom right panel IAS is shown, which quantifies the level of agreement (or disagreement)  
among the various satellite input data sets. The IAS maps also shows the location of the TCCON sites (pink triangles) and  
the IAS values at the TCCON sites (see pink triangles above the colour bar). As can be seen, the TCCON sites are typically  
located outside of regions where the IAS is highest.

310 The average IAS for the entire time period 2003-2018 is shown in Fig. 9. As can be seen, the scatter is typically in the range  
0.6-1.1 ppm with the exception of parts of the tropics, in particular central Africa, parts of south-east Asia and high latitudes.  
High latitudes typically correspond to large solar zenith angles, which is a challenge for accurate satellite XCO<sub>2</sub> retrievals, as  
this typically corresponds to low signal and therefore low signal-to-noise resulting in enhanced scatter of the retrieved XCO<sub>2</sub>.  
In areas with frequent cloud coverage, such as parts of the tropics, sampling is sparse and this may also contribute to a larger  
315 scatter.

The comparison of the various XCO<sub>2</sub> data products with TCCON XCO<sub>2</sub> at 10 TCCON sites is shown in Fig. 10. These 10  
TCCON sites fulfil the EMMA criteria in terms of a sufficiently large number of collocations as defined to obtain robust  
conclusions per site. The individual soundings of the EMMA XCO<sub>2</sub> product are shown as white circles with black border. As  
can be seen, they are located within (mostly close to the centre) of the range of values of the individual sensor/algorithm



320 XCO<sub>2</sub> values, which is expected. The validation results are summarized in Tab. 4 (per site) and Tab. 5 (overall) together with the corresponding results of the QA/QC assessment method.

Table 4 lists all TCCON sites, which fulfil either the EMMA method or the QA/QC method criteria with respect to minimum number of collocations and length of time series. Listed are the numerical values (in ppm), which have been computed for several figures of merit. This includes (i) the overall estimation of the single observation random error computed as standard  
325 deviation of the satellite minus TCCON differences, (ii) the uncertainty ratio, which is the ratio of the mean value of the reported (1-sigma) uncertainty to the standard deviation of the satellite – TCCON difference (computed to validate the reported uncertainties), (iii) the overall bias computed as the mean value of the satellite – TCCON differences and (iv) the seasonal bias, computed as the standard deviation of the biases determined for the four seasons. Also shown in the last two rows are the mean value and the standard deviation of the values listed per TCCON site in the rows above. Several of these  
330 values have been used to compute the values listed in Tab. 5, which shows the overall summary of the quality assessment.

Table 5 lists (i) the mean value of the single observation random error, (ii) the global bias computed as the mean value of the biases at the various TCCON sites, (iii) the regional bias computed as the standard deviation of the biases at the various TCCON sites, (iv) the mean seasonal bias and (v) the spatio-temporal bias computed as the root-sum-square of the regional and of the seasonal bias. The spatio-temporal bias is used to quantify the achieved performance for “relative accuracy”,  
335 which characterizes the spatially and temporally varying component of the bias (i.e., neglects a possible global bias (global offset), which is reported separately).

The linear bias trend has also been computed by fitting a line to the satellite – TCCON differences (not shown here). The mean value of the linear trend (slope) and its uncertainty (1-sigma, obtained from the standard deviation of the slope at the various TCCON sites) are  $-0.05 \pm 0.06$  ppm/year for the EMMA method and  $-0.06 \pm 0.09$  ppm/year for the QA/QC method.  
340 This means that no significant long-term bias trend has been detected, i.e., the satellite product is stable.

As can be seen from Tab. 5, the values computed independently using the EMMA and the QA/QC assessment methods are quite similar, which gives not only confidence in the overall quality assessment summary documented in Tab. 5 but also in the products and the used validation methods.

Note however that the quality of the satellite data (at least at TCCON sites) is very likely better than Tab. 5 suggests because  
345 (i) the TCCON retrievals are not free of errors (the 1-sigma XCO<sub>2</sub> uncertainty is about 0.4 ppm (Wunch et al., 2010)) and (ii) because of the representation error originating from the (real) spatio-temporal variability of XCO<sub>2</sub> around the TCCON sites. The overall error related to this is difficult to quantify but some indication can potentially be obtained by additional assessment results such as the one shown in Fig. 11. Figure 11 shows the biases as obtained with the EMMA method at the various TCCON sites used for the EMMA method comparisons. Shown are not only the mean satellite – TCCON differences  
350 as obtained for the EMMA product but also for all the individual sensor/algorithm input products. The differences are shown as anomalies with respect to the mean, i.e., the sum of the differences in each row is zero. This is equivalent to assuming that



for a given satellite product the mean value over all TCCON sites is zero. As can be seen from Fig. 11, the satellite – TCCON differences are dominantly positive (orange and red colours) for higher latitude TCCON sites and mostly negative (blue colours) for lower latitude TCCON sites. In order to rule out that this is an artefact of the EMMA assessment method, the overall biases computed with the QA/QC method and biases computed by the individual product data providers (DPs) have also been derived. These biases have been used to compute - for each of the 10 TCCON sites shown in Fig. 11 - the mean bias and the standard deviation of these biases. For 4 of these 10 sites the mean bias is considerably (more than 1.5 times) larger than the standard deviation of the biases and the corresponding results for these 4 sites are shown in Tab. 6. This does not necessarily mean, that these sites have the largest biases but only that the biases (independent of their magnitude) are most consistent at these sites. As can be seen from Tab. 6, the biases are always positive at Sodankylä, Karlsruhe and Orléans and always negative at Lamont. Because it is unlikely that all three satellites and several retrieval algorithms produce XCO<sub>2</sub> products with similar biases at a given TCCON sites, this provides an indication of biases either due to representation errors or due to biases within the TCCON data (Tab. 6). Note that these biases are within the accuracy stated by TCCON, which is 0.8 ppm (2-sigma) (Wunch et al., 2010, Hedelius et al., 2017). The accuracy of the TCCON data will be improved for the next data release (planned for 2020). This new TCCON dataset will allow for better identification of the causes for the observed biases.

The XCO<sub>2</sub>\_OBS4MIPS product has also been directly compared with TCCON using a comparison method based on the comparison of the monthly satellite product with TCCON monthly mean values. The results are shown in Fig. 12. As can be seen, the mean difference (satellite - TCCON) is 0.18 ppm (which is close to the mean value of the global bias of 0.20 ppm listed in Tab. 5), the standard deviation is 1.18 ppm (as expected (because of the spatio-temporal averaging) somewhat smaller than the value obtained for the XCO<sub>2</sub>\_EMMA product (1.29 ppm) listed in Tab. 5) and the linear correlation coefficient is 0.99. The spatio-temporal bias, computed as the standard deviation of 3-monthly averages at the TCCON sites listed in Fig. 12, is 0.7 ppm.

Figure 1 presents an overview of the XCO<sub>2</sub> data product in terms of time series for three latitude bands and global maps. XCO<sub>2</sub> is increasing almost linearly during the 16 year time period (for a discussion of the derived annual growth rates see Sect. 4.3). The main reason for this increase is CO<sub>2</sub> emission due to burning of fossil fuels (Le Quéré et al., 2018). The seasonal cycle, which is caused primarily by quasi-regular uptake and release of atmospheric CO<sub>2</sub> by the terrestrial vegetation due to photosynthesis and respiration (e.g., Kaminski et al., 2017, Yin et al., 2018) is most pronounced over the northern hemisphere. The half-yearly maps for 2003 are based on SCIAMACHY onboard ENVISAT (Burrows et al., 1995; Bovensmann et al., 1999) satellite data and the maps for 2018 contain data from the GOSAT (since 2009) (Kuze et al., 2016) and OCO-2 (since 2014) (Crisp et al., 2004) satellites. GOSAT and OCO-2 also provide good-quality XCO<sub>2</sub> retrievals over the oceans due to their sun-glint observation mode. The XCO<sub>2</sub> retrievals are based on spectra of reflected solar radiation in the Short-Wave-Infra-Red (SWIR) spectral region (around 1.6 and 2.0 μm). In this spectral region water is a poor reflector of



385 solar radiation. Good signal - and therefore also a high signal-to-noise ratio - typically requires sun-glint tracking, which is an observation mode implemented for GOSAT and OCO-2 but for SCIAMACHY.

#### 4.2 Products XCH<sub>4</sub>\_EMMA and XCH<sub>4</sub>\_OBS4MIPS (v4.1)

As for XCO<sub>2</sub>, monthly maps have also been generated for the EMMA XCH<sub>4</sub> data product. Two examples are shown in Fig. 13 for September 2010 and in Fig. 14 for September 2018. The individual sensor XCH<sub>4</sub> input data are shown in the first four rows and the EMMA XCH<sub>4</sub> product is shown in the bottom left panel. The bottom right panel shows the IAS. As can be seen, the spatial pattern of the XCH<sub>4</sub> maps are similar but not identical. The IAS shows a quite large variability. The “scatter” is larger compared to the corresponding XCO<sub>2</sub> IAS (Figs. 7 and 8, bottom right panels) and spatially the grid cells with larger spread are more equally distributed over the globe but with largest differences over the southern part of Asia.

Figure 15 shows the comparison of the EMMA XCH<sub>4</sub> product (white circles with black border) and of the individual sensor XCH<sub>4</sub> input products with TCCON XCH<sub>4</sub> originating from the EMMA assessment method. As for the EMMA XCO<sub>2</sub> product (Fig. 10), the EMMA XCH<sub>4</sub> is located near the center of the “clouds of XCH<sub>4</sub> values”, as expected. The validation results are summarized in Tabs. 7 and 8, which have the same structure as the corresponding XCO<sub>2</sub> tables (Tabs. 4 and 5). These tables also list the results of the QA/QC assessment method, which results in quite similar (within a few ppb) overall quality assessment results (Tab. 8) as obtained with the EMMA method. The linear bias trend has also been computed by fitting a line to the satellite – TCCON differences (not shown here). The mean value of the linear trend (slope) and its uncertainty (1-sigma, obtained from the standard deviation of the slope at the various TCCON sites) are  $-0.1 \pm 0.4$  ppb/year for the EMMA method and  $0.5 \pm 0.8$  ppb/year for the QA/QC method. As for XCO<sub>2</sub>, this means that no significant long-term bias trend has been detected, i.e., the satellite product is stable.

The XCH<sub>4</sub>\_OBS4MIPS product has also been directly compared with TCCON (Fig. 16) using the same method as also used for product XCO<sub>2</sub>\_OBS4MIPS (Fig. 12). As can be seen from Fig. 16, the mean difference (satellite - TCCON) is -2.88 ppb (which is close to the mean value of the global bias of -2.0 ppb of product XCH<sub>4</sub>\_EMMA listed in Tab. 8), the standard deviation is 8.65 ppb (as expected (because of the averaging) somewhat smaller than the value of 17.4 ppb obtained for the XCH<sub>4</sub>\_EMMA product listed in Tab. 8) and the linear correlation coefficient is 0.97.

Figure 2 presents an overview of the XCH<sub>4</sub> data product in terms of time series for three latitude bands and global maps. As can be seen, XCH<sub>4</sub> was nearly constant during 2003-2006 (apart from seasonal fluctuations) but is increasing since 2007 (for a discussion of the trend and annual growth rates see Sect. 4.3). The reason for this is likely a combination of increasing natural (e.g., wetlands) and anthropogenic (e.g., fossil fuel related) emissions and possibly decreasing sinks (hydroxyl (OH) radical) but it seems currently not to be possible to be more definitive (e.g., Worden et al., 2017; Nisbet et al., 2019; Turner et al., 2019; Howarth, 2019; Schaefer, 2019).



415

### 4.3 Annual growth rates

Finally, we present an update and extension of the year 2003-2016 annual XCO<sub>2</sub> growth rates shown in Buchwitz et al., 2018, using the new OBS4MIPS v4.1 XCO<sub>2</sub> data set covering the time period 2003-2018 (Fig. 17). Figure 17(a) shows the time series of the globally averaged OBS4MIPS version 4.1 XCO<sub>2</sub> data product over land. In contrast to Buchwitz et al., 2018, the analysis presented here is based on data over land only as this permits to generate a time series with better internal consistency (note that the XCO<sub>2</sub> OBS4MIPS product is land only for 2003-2008). The average growth rate during 2010-2018, i.e., for the time period where an ensemble of GOSAT and OCO-2 data has been used, is  $2.28 \pm 0.04$  ppm/year. As can be seen from Fig. 17(b), the year 2017 and 2018 growth rates are less than the growth rates of the years 2015 and 2016, which were years with a strong El Niño. The XCO<sub>2</sub> growth rates are in reasonable agreement with the global CO<sub>2</sub> growth rates published by National Oceanic and Atmospheric Administration (NOAA) (shown in blue colour in Fig. 17(b)), which are based on marine surface CO<sub>2</sub> observations ([ftp://aftp.cmdl.noaa.gov/products/trends/co2/co2\\_gr\\_gl.txt](ftp://aftp.cmdl.noaa.gov/products/trends/co2/co2_gr_gl.txt); last access: 30-July-2019). As can be seen from Fig. 17(b), the agreement of the satellite-derived XCO<sub>2</sub> growth rates with the NOAA surface CO<sub>2</sub> based growth rates is better from year 2010 onwards compared to the time period before when the EMMA data set consists only of one SCIAMACHY data set instead of the full ensemble. For 2018, the XCO<sub>2</sub> growth rate is  $2.1 \pm 0.5$  ppm/year, which is lower than the NOAA surface CO<sub>2</sub> growth rate of  $2.43 \pm 0.08$  ppm/year. Note that the 1-sigma uncertainty ranges of the two growth rate estimates overlap, which indicates that the two growth rate estimates are consistent.

The growth rate of atmospheric methane is also an important quantity (e.g., Nisbet et al., 2019). The method of Buchwitz et al., 2018, has now also been used to compute annual XCH<sub>4</sub> growth rates from satellite XCH<sub>4</sub> retrievals. Figure 18(a) shows the time series of the globally averaged OBS4MIPS version 4.1 XCH<sub>4</sub> data product over land. As shown by the linear fit, the average growth rate is  $7.9 \pm 0.2$  ppb/year during 2010-2018, i.e., for the time period where an ensemble of GOSAT data has been used. The annual growth rates are shown in Fig. 18(b) for the satellite-derived XCH<sub>4</sub> (red) and for the NOAA growth rates ([ftp://aftp.cmdl.noaa.gov/products/trends/ch4/ch4\\_gr\\_gl.txt](ftp://aftp.cmdl.noaa.gov/products/trends/ch4/ch4_gr_gl.txt); last access: 30-July-2019) derived from marine surface CH<sub>4</sub> observations. For 2018, the XCH<sub>4</sub> growth rate is  $10 \pm 6$  ppb/year, which is close to the NOAA surface CH<sub>4</sub> growth rate of  $9.46 \pm 0.56$  ppb/year.

### 5 Summary and conclusions

Satellite-derived ensemble XCO<sub>2</sub> and XCH<sub>4</sub> data products have been generated and validated. These data products are the version 4.1 Level 2 (L2) products XCO<sub>2</sub>\_EMMA and XCH<sub>4</sub>\_EMMA and the Level 3 (L3) products XCO<sub>2</sub>\_OBS4MIPS and XCH<sub>4</sub>\_OBS4MIPS and cover the time period 2003-2018. The data products are freely available for interested users via the Copernicus Climate Data Store (CDS, <https://cds.climate.copernicus.eu/>), where also earlier versions of these data products





are accessible. The L2 products have been generated with an adapted version of the EMMA algorithm (Reuter et al., 2013) and the L3 products have been generated by gridding (averaging) the EMMA L2 product to obtain products at monthly time and 5°x5° spatial resolution in Obs4MIPS format. The products have been validated by comparisons with TCCON ground-based XCO<sub>2</sub> and XCH<sub>4</sub> retrievals using TCCON version GGG2014.

From January 2003 – March 2009 the products are based on SCIAMACHY/ENVISAT and from April 2009 onwards using an ensemble of one SCIAMACHY (until early 2012) and several GOSAT products. The XCO<sub>2</sub> products contain in addition L2 products from NASA's OCO-2 mission from 09/2014 onwards.

The EMMA algorithm selects for each month and each 10°x10° grid cell one of the available products, i.e., one from the existing ensemble of L2 input products, and transfers all relevant information (including averaging kernel etc.) from the selected L2 input product into the merged EMMA L2 product. The selected product is the “median product”. The main purpose of EMMA is to generate a Level 2 product, which covers an as long as possible time series (longer than any of the individual sensor input data sets) with as high as possible accuracy including all information needed, e.g., for surface flux inverse modelling. The “median approach” helps to reduce the occurrence of potential outliers and thus reduces spatial and temporal biases in the generated data products.

Detailed quality assessment results based on comparisons with TCCON ground-based retrievals have been presented. We found that the XCO<sub>2</sub> Level 2 data set at the TCCON validation sites can be characterized by the following figures of merit (the corresponding values for the Level 3 product are listed in brackets): single observation random error (1-sigma): 1.29 ppm (monthly: 1.18 ppm); global bias: 0.20 ppm (0.18 ppm), spatio-temporal bias or “relative accuracy” (1-sigma): 0.66 ppm (0.70 ppm). The corresponding values for the XCH<sub>4</sub> products are: single observation random error (1-sigma): 17.4 ppb (monthly: 8.7 ppb); global bias: -2.0 ppb (-2.9 ppb), spatio-temporal bias (1-sigma): 5.0 ppb (4.9 ppb). It has also been found that the data products exhibit very good long-term stability as no significant linear bias trends have been identified.

The new data sets have also been used to derive annual XCO<sub>2</sub> and XCH<sub>4</sub> growth rates, which are in reasonable to good agreement with growth rates from the National Oceanic and Atmospheric Administration (NOAA) based on marine surface observations.

An important application for the EMMA products is to use them together with inverse modelling to obtain improved information on regional scale CO<sub>2</sub> (e.g., Houweling et al., 2015) and CH<sub>4</sub> (e.g., Alexe et al., 2015) surface fluxes. Applications for the corresponding OBS4MIPS products are, for example, climate model comparisons (e.g., Lauer et al., 2017) and studies related to annual growth rates (e.g., Buchwitz et al., 2018). It is however important to note that these merged products are not necessarily the most optimal products for all applications as they do not contain all data from a given satellite sensor. For example, users interested primarily in emissions from power plants or other localized CO<sub>2</sub> sources will prefer the original OCO-2 Level 2 data product (e.g., Nassar et al., 2017; Reuter et al., 2019a). Especially for users



interested in only parts of the time series it is recommended to use the individual sensor products in addition to the merged product as this may significantly increase the robustness, reliability and uncertainty characterization of key findings.

480

## Acknowledgements

The generation of the EMMA Level 2 and OBS4MIPS Level 3 data sets and the corresponding data analysis has been funded primarily by the European Union (EU) via the Copernicus Climate Change Service (C3S, <https://climate.copernicus.eu/>) managed by the European Centre for Medium-range Weather Forecasts (ECMWF).

485

The work presented here strongly benefited from additional funding by the European Space Agency (ESA) via ESA's Climate Change Initiative (CCI, <http://www.esa-ghg-cci.org/>) projects GHG-CCI/GHG-CCI+.

The further development of the FOCAL retrieval algorithm used to generate the OCO-2/FOCAL XCO<sub>2</sub> input data product would not have been possible without co-funding from the EU H2020 projects CHE (Grant Agreement No. 776186) and VERIFY (Grant Agreement No. 776810). The generation of the XCO<sub>2</sub>\_OBS4MIPS product also benefited from co-funding from EU H2020 project CCiCC (Grant Agreement No. 821003).

490

We thank several space agencies for making available satellite Level 1 (L1) input data: ESA/DLR for SCIAMACHY L1 data, JAXA for GOSAT Level 1B data and NASA for the OCO-2 L1 data product. We also thank ESA for making the GOSAT L1 product available via the ESA Third Party Mission (TPM) archive.

495 We thank NIES for the operational GOSAT XCO<sub>2</sub> and XCH<sub>4</sub> Level 2 products (obtained from <https://data2.gosat.nies.go.jp/>, last access: 4-September-2019) and the NASA team for the GOSAT and OCO-2 ACOS Level 2 XCO<sub>2</sub> products (the NASA GOSAT L2 data product has been obtained from

[https://oco2.gesdisc.eosdis.nasa.gov/data/GOSAT\\_TANSO\\_Level2/ACOS\\_L2\\_Lite\\_FP.7.3/](https://oco2.gesdisc.eosdis.nasa.gov/data/GOSAT_TANSO_Level2/ACOS_L2_Lite_FP.7.3/), last access: 4-September-2019; the NASA OCO-2 data product has been obtained from

500 [https://oco2.gesdisc.eosdis.nasa.gov/data/s4pa/OCO2\\_DATA/OCO2\\_L2\\_Lite\\_FP.9r/](https://oco2.gesdisc.eosdis.nasa.gov/data/s4pa/OCO2_DATA/OCO2_L2_Lite_FP.9r/), last access: 4-September-2019).

TCCON data were obtained from the TCCON Data Archive, hosted by CaltechDATA, California Institute of Technology (<https://tccondata.org/>, last access: 15-July-2019).

The TCCON stations Ascension Island, Bremen, Garmisch, Karlsruhe and Ny-Ålesund have been supported by the German Bundesministerium für Wirtschaft und Energie (BMWi) via DLR under grants 50EE1711A-E. We thank the ESA Ariane Tracking Station at North East Bay, Ascension Island, for hosting and local support. N.M.D. is supported by an ARC Future Fellowship, FT180100327.

505

We also thank NOAA for access to the surface CO<sub>2</sub> (file [ftp://aftp.cmdl.noaa.gov/products/trends/co2/co2\\_gr\\_gl.txt](ftp://aftp.cmdl.noaa.gov/products/trends/co2/co2_gr_gl.txt); last access: 30-July-2019) and CH<sub>4</sub> (file [ftp://aftp.cmdl.noaa.gov/products/trends/ch4/ch4\\_gr\\_gl.txt](ftp://aftp.cmdl.noaa.gov/products/trends/ch4/ch4_gr_gl.txt); last access: 30-July-2019)



510 growth rate data sets. Output from NOAA's CarbonTracker has been used as input for the SECM2018 model.  
CarbonTracker CT2017 results provided by NOAA ESRL, Boulder, Colorado, USA from the website at  
<http://carbontracker.noaa.gov/> (last access: 4-September-2019).

We also thank Peter Bergamaschi for providing MACC-II project inversion system CH<sub>4</sub> fields, which have been used as  
input for the SC4C2018 model.

### 515 **Author contributions**

M.R. generated the EMMA and OBS4MIPS XCO<sub>2</sub> and XCH<sub>4</sub> version 4.1 data sets. M.R. and M.B. have performed the data  
analysis. M.B. has written the first version of the paper with support of M.R. The following authors have provided input data  
or expertise on data sets: M.R., M.B., O.S., S.N., H.B., J.P.B., H.Boe., A.D.N., J.A., R.J.P., P.S., L.W., O.P.H., I.A., A.K.,  
H.S., K.S., Y.Y., I.M., D.C., C.W.O'D., J.N., C.P., T.W., V.A.V., N.M.D., D.W.T.G., R.K., D.P., F.H., R.S., Y.V.T., K.S.,  
520 S.R., M.K.S., M.D.M., D.G.F., L.T.I., C.M.R., C.R., D.S. All authors contributed to significantly improve the manuscript.

**Data availability.** The EMMA and OBS4MIPS XCO<sub>2</sub> and XCH<sub>4</sub> version 4.1 data products (but also several data sets used  
as input, see data sets with "CCI/C3S product ID" in Tabs. 1 and 2) are available (from December 2019 onwards) via the  
Copernicus Climate Change Service (C3S, <https://climate.copernicus.eu/>) Climate Data Store (CDS,  
525 <https://cds.climate.copernicus.eu/>) including documentation such as the product user guides (Buchwitz et al., 2019c; Reuter  
et al., 2019d).

### **Competing financial interests**

The authors declare no competing financial interests.

530



## References

- Alexe, M., Bergamaschi, P., Segers, A., Detmers, R., Butz, A., Hasekamp, O., Guerlet, S., Parker, R., Boesch, H., Frankenberg, C., Scheepmaker, R. A., Dlugokencky, E., Sweeney, C., Wofsy, S. C., and Kort, E. A.: Inverse modeling of CH<sub>4</sub> emissions for 2010–2011 using different satellite retrieval products from GOSAT and SCIAMACHY, *Atmos. Chem. Phys.*, 15, 113–133, [www.atmos-chem-phys.net/15/113/2015/](http://www.atmos-chem-phys.net/15/113/2015/), doi:10.5194/acp-15-113-2015, 2015.
- Basu, S., Guerlet, S., Butz, A., Houweling, S., Hasekamp, O., Aben, I., Krummel, P., Steele, P., Langenfelds, R., Torn, M., Biraud, S., Stephens, B., Andrews, A., and Worthy, D.: Global CO<sub>2</sub> fluxes estimated from GOSAT retrievals of total column CO<sub>2</sub>, *Atmos. Chem. Phys.*, 13, 8695–8717, doi:10.5194/acp-13-8695-2013, 2013.
- 535 Bovensmann, H., Burrows, J. P., Buchwitz, M., Frerick, J., Noël, S., Rozanov, V. V., Chance, K. V., and Goede, A. H. P.: SCIAMACHY - Mission objectives and measurement modes, *J. Atmos. Sci.*, 56 (2), 127-150, 1999.
- Boesch, H., Anand, J., Di Noia, A., Buchwitz, M., Somkuti, P., and Parker, R.: Product Quality Assessment Report (PQAR) – ANNEX A for products CO<sub>2</sub>\_GOS\_OCFP, CH<sub>4</sub>\_GOS\_OCFP & CH<sub>4</sub>\_GOS\_OCPR (v7.2, 2009-2018), Technical Report Copernicus Climate Change Service (C3S), version 3.0, 12-08-2019, pp. 44, access: available in December 2019 from CDS website (<https://cds.climate.copernicus.eu>), 2019.
- 545 Bril, A., Oshchepkov, S., and Yokota, T.: Application of a probability density function-based atmospheric light-scattering correction to carbon dioxide retrievals from GOSAT over-sea observations. *Remote Sensing of the Environment* 2012, 117, 301–306, 2012.
- Buchwitz, M., Reuter, M., Schneising, O., Boesch, H., Guerlet, S., Dils, B., Aben, I., Armante, R., Bergamaschi, P., Blumenstock, T., Bovensmann, H., Brunner, D., Buchmann, B., Burrows, J. P., Butz, A., Chédin, A., Chevallier, F., Crevoisier, C. D., Deutscher, N. M., Frankenberg, C., Hase, F., Hasekamp, O. P., Heymann, J., Kaminski, T., Laeng, A., Lichtenberg, G., De Mazière, M., Noël, S., Notholt, J., Orphal, J., Popp, C., Parker, R., Scholze, M., Sussmann, R., Stiller, G. P., Warneke, T., Zehner, C., Bril, A., Crisp, D., Griffith, D. W. T., Kuze, A., O’Dell, C., Oshchepkov, S., Sherlock, V., Suto, H., Wennberg, P., Wunch, D., Yokota, T., and Yoshida, Y.: The Greenhouse Gas Climate Change Initiative (GHG-CCI): comparison and quality assessment of near-surface-sensitive satellite-derived CO<sub>2</sub> and CH<sub>4</sub> global data sets, *Remote Sensing of Environment*, 162, 344-362, doi:10.1016/j.rse.2013.04.024, 2015.
- 555 Buchwitz, M., Schneising, O., Reuter, M., Heymann, J., Krautwurst, S., Bovensmann, H., Burrows, J. P., Boesch, H., Parker, R. J., Somkuti, P., Detmers, R. G., Hasekamp, O. P., Aben, I., Butz, A., Frankenberg, C., Turner, A. J., Satellite-derived methane hotspot emission estimates using a fast data-driven method, *Atmos. Chem. Phys.*, 17, 5751-5774, doi:10.5194/acp-17-5751-2017, 2017a.
- 560



- 565 Buchwitz, M., Reuter, M., Schneising, O., Hewson, W., Detmers, R. G., Boesch, H., Hasekamp, O. P., Aben, I., Bovensmann, H., Burrows, J. P., Butz, A., Chevallier, F., Dils, B., Frankenberg, C., Heymann, J., Lichtenberg, G., De Maziere, M., Notholt, J., Parker, R., Warneke, T., Zehner, C., Griffith, D. W. T., Deutscher, N. M., Kuze, A., Suto, H., and Wunch, D.: Global satellite observations of column-averaged carbon dioxide and methane: The GHG-CCI XCO<sub>2</sub> and XCH<sub>4</sub> CRDP3 data set, *Remote Sensing of Environment* 203, 276-295, <http://dx.doi.org/10.1016/j.rse.2016.12.027>, 2017b.
- Buchwitz, M., Reuter, M., Schneising, O., Noel, S., Gier, B., Bovensmann, H., Burrows, J. P., Boesch, H., Anand, J., Parker, R. J., Somkuti, P., Detmers, R. G., Hasekamp, O. P., Aben, I., Butz, A., Kuze, A., Suto, H., Yoshida, Y., Crisp, D., and O'Dell, C.: Computation and analysis of atmospheric carbon dioxide annual mean growth rates from satellite observations during 2003-2016, *Atmos. Chem. Phys.*, 18, 17355-17370, <https://doi.org/10.5194/acp-18-17355-2018>, 2018.
- 570 Buchwitz, M., Reuter, M., Schneising-Weigel, O., Aben, I., Wu, L., Hasekamp, O. P., Boesch, H., Di Noia, A., Crevoisier, C. and Armante, R.: Product Quality Assessment Report (PQAR) – Main document for Greenhouse Gas (GHG: CO<sub>2</sub> & CH<sub>4</sub>) data set CDR 3 (2003-2018), Technical Report Copernicus Climate Change Service (C3S), version 3.0, 12-08-2019, pp. 103, access: available in December 2019 from CDS website (<https://cds.climate.copernicus.eu>), 2019a.
- Buchwitz, M., Reuter, M., Schneising-Weigel, O., Aben, I., Wu, L., Hasekamp, O. P., Boesch, H., Di Noia, A., Crevoisier, C. and Armante, R.: Algorithm Theoretical Basis Document (ATBD) – Main document for Greenhouse Gas (GHG: CO<sub>2</sub> & CH<sub>4</sub>) data set CDR 3 (2003-2018), Technical Report Copernicus Climate Change Service (C3S) (main document and 5 Annexes), version 3.0, 12-08-2019, pp. 43, access: available in December 2019 from CDS website (<https://cds.climate.copernicus.eu>), 2019b.
- 580 Buchwitz, M., Reuter, M., Schneising-Weigel, O., Aben, I., Wu, L., Hasekamp, O. P., Boesch, H., Di Noia, A., Crevoisier, C. and Armante, R.: Product User Guide and Specification (PUGS) – Main document for Greenhouse Gas (GHG: CO<sub>2</sub> & CH<sub>4</sub>) data set CDR 3 (2003-2018), Technical Report Copernicus Climate Change Service (C3S), version 3.0, 12-08-2019, pp. 97, access: available in December 2019 from CDS website (<https://cds.climate.copernicus.eu>), 2019c.
- Burrows, J. P., Hölzle, E., Goede, A. P. H., Visser, H., and Fricke, W.: SCIAMACHY—Scanning Imaging Absorption Spectrometer for Atmospheric Chartography, *Acta Astronaut.*, 35(7), 445–451, doi:10.1016/0094-5765(94)00278-t, 1995.
- 585 Butz, A., Hasekamp, O.P., Frankenberg, C., Vidot, J., and Aben, I.: CH<sub>4</sub> retrievals from space-based solar backscatter measurements: Performance evaluation against simulated aerosol and cirrus loaded scenes, *J. Geophys. Res.*, VOL. 115, D24302, doi:10.1029/2010JD014514. 2010.
- Butz, A., Guerlet, S., Hasekamp, O., Schepers, D., Galli, A., Aben, I., Frankenberg, C., Hartmann, J.-M., Tran, H., Kuze, A., Keppel-Aleks, G., Toon, G., Wunch, D., Wennberg, P., Deutscher, N., Griffith, D., Macatangay, R., Messerschmidt, J., Notholt, J., and Warneke, T.: Toward accurate CO<sub>2</sub> and CH<sub>4</sub> observations from GOSAT, *Geophys. Res. Lett.*, doi:10.1029/2011GL047888, 2011.
- 590



- Chevallier, F., Palmer, P. I., Feng, L., Boesch, H., O'Dell, C. W., and Bousquet, P.: Towards robust and consistent regional CO<sub>2</sub> flux estimates from in situ and space-borne measurements of atmospheric CO<sub>2</sub>, *Geophys. Res. Lett.*, 41, 1065–1070, doi:10.1002/2013GL058772, 2014.
- 595 Chevallier, F.: On the statistical optimality of CO<sub>2</sub> atmospheric inversions assimilating CO<sub>2</sub> column retrievals, *Atmos. Chem. Phys.*, 15, 11133–11145, <https://doi.org/10.5194/acp-15-11133-2015>, 2015.
- Cogan, A. J., Boesch, H., Parker, R. J., Feng, L., Palmer, P. I., Blavier, J.-F. L., Deutscher, N. M., Macatangay, R., Notholt, J., Roehl, C., Warneke, T., and Wunsch, D.: Atmospheric carbon dioxide retrieved from the Greenhouse gases Observing SATellite (GOSAT): Comparison with ground-based TCCON observations and GEOS-Chem model calculations, *J. Geophys. Res.*, 117, D21301, doi:10.1029/2012JD018087, 2012.
- 600 Crisp, D., Atlas, R. M., Bréon, F.-M., Brown, L. R., Burrows, J. P., Ciais, P., Connor, B. J., Doney, S. C., Fung, I. Y., Jacob, D. J., Miller, C. E., O'Brien, D., Pawson, S., Randerson, J. T., Rayner, P., Salawitch, R. S., Sander, S. P., Sen, B., Stephens, G. L., Tans, P. P., Toon, G. C., Wennberg, P. O., Wofsy, S. C., Yung, Y. L., Kuang, Z., Chudasama, B., Sprague, G., Weiss, P., Pollock, R., Kenyon, D., and Schroll, S.: The Orbiting Carbon Observatory (OCO) mission, *Advances in Space Research*, 34, 700–709, 2004.
- 605 De Mazière, M., Sha, M. K., Desmet, F., Hermans, C., Scolas, F., Kumps, N., Metzger, J.-M., Dufлот, V., and Cammas, J.-P.: TCCON data from Réunion Island (RE), Release GGG2014R1. TCCON data archive, hosted by CaltechDATA, <https://doi.org/10.14291/tcon.ggg2014.reunion01.R1>, 2017.
- Deutscher, N. M., Notholt, J., Messerschmidt, J., Weinzierl, C., Warneke, T., Petri, C., Grupe, P., and Katrynski, K.: TCCON data from Białystok (PL), Release GGG2014R2. TCCON data archive, hosted by CaltechDATA, <https://doi.org/10.14291/tcon.ggg2014.bialystok01.R2>, 2019.
- 610 Dils, B., Buchwitz, M., Reuter, M., Schneising, O., Boesch, H., Parker, R., Guerlet, S., Aben, I., Blumenstock, T., Burrows, J. P., Butz, A., Deutscher, N. M., Frankenberg, C., Hase, F., Hasekamp, O. P., Heymann, J., De Mazière, M., Notholt, J., Sussmann, R., Warneke, T., Griffith, D., Sherlock, V., and Wunch, D.: The Greenhouse Gas Climate Change Initiative (GHG-CCI): comparative validation of GHG-CCI SCIAMACHY/ENVISAT and TANSO-FTS/GOSAT CO<sub>2</sub> and CH<sub>4</sub> retrieval algorithm products with measurements from the TCCON, *Atmos. Meas. Tech.*, 7, 1723–1744, 2014.
- Feist, D. G., Arnold, S. G., John, N., and Geibel, M. C.: TCCON data from Ascension Island (SH), Release GGG2014R0. TCCON data archive, hosted by CaltechDATA, <https://doi.org/10.14291/tcon.ggg2014.ascension01.R0/1149285>, 2014.
- 620 Ganesan, A. L., Rigby, M., Lunt, M. F., Parker, R. J., Boesch, H., Goulding, N., Umezawa, T., Zahn, A., Chatterjee, A., Prinn, R. G., Tiwari, Y. K., van der Schoot, M., and Krummel, P. B.: Atmospheric observations show accurate reporting and little growth in India's methane emissions, *Nature Communications*, volume 8, article number: 836, 2017.





Gaubert, B., Stephens, B. B., Basu, S., Chevallier, F., Deng, F., Kort, E. A., Patra, P. K., Peters, W., Rödenbeck, C., Saeki, T., Schimel, D., Van der Laan-Luijkx, I., Wofsy, S., and Yin, Y.: Global atmospheric CO<sub>2</sub> inverse models converging on neutral tropical land exchange, but disagreeing on fossil fuel and atmospheric growth rate, *Biogeosciences*, 16, 117-134, 625 <https://doi.org/10.5194/bg-16-117-2019>, 2019.

GCOS-154: Global Climate Observing System (GCOS), SYSTEMATIC OBSERVATION REQUIREMENTS FOR SATELLITE-BASED PRODUCTS FOR CLIMATE, Supplemental details to the satellite-based component of the “Implementation Plan for the Global Observing System for Climate in Support of the UNFCCC (2010 update)”, Prepared by World Meteorological Organization (WMO), Intergovernmental Oceanographic Commission, United Nations Environment 630 Programme (UNEP), International Council for Science, Doc.: GCOS 154, link: <https://www.wmo.int/pages/prog/gcos/Publications/gcos-154.pdf> (last access: 21-February-2019), 2010.

GCOS-200: The Global Observing System for Climate: Implementation Needs, World Meteorological Organization (WMO), GCOS-200 (GOOS-214), pp. 325, link: [http://unfccc.int/files/science/workstreams/systematic\\_observation/application/pdf/gcos\\_ip\\_10oct2016.pdf](http://unfccc.int/files/science/workstreams/systematic_observation/application/pdf/gcos_ip_10oct2016.pdf) (last access: 21- 635 February-2019), 2016.

Griffith, D. W., Velazco, V. A., Deutscher, N. M., Murphy, C., Jones, N. B., Wilson, S. R., Macatangay, R. C., Kettlewell, G. C., Buchholz, R. R., and Riggenbach, M. O.: TCCON data from Wollongong, (AU), Release GGG2014R0. TCCON data archive, hosted by Caltech-DATA, <https://doi.org/10.14291/tcon.ggg2014.wollongong01.R0/1149291>, 2014a.

Griffith, D.W. T., Deutscher, N. M., Velazco, V. A., Wennberg, P. O., Yavin, Y., Keppel-Aleks, G., Washenfelder, R. A., 640 Toon, G. C., Blavier, J.-F., Murphy, C., Jones, N. B., Kettlewell, G. C., Connor, B. J., Macatangay, R. C., Roehl, C., Ryzek, M., Glowacki, J., Culgan, T., and Bryant, G. W.: TCCON data from Darwin (AU), Release GGG2014R0. TCCON data archive, hosted by CaltechDATA, <https://doi.org/10.14291/tcon.ggg2014.darwin01.R0/1149290>, 2014b.

Hase, F., Blumenstock, T., Dohe, S., Groß, J., and Kiel, M.: TCCON data from Karlsruhe (DE), Release GGG2014R1. TCCON data archive, hosted by CaltechDATA, <https://doi.org/10.14291/tcon.ggg2014.karlsruhe01.R1/1182416>, 2015.

645 Hayman, G. D., O'Connor, F. M., Dalvi, M., Clark, D. B., Gedney, N., Huntingford, C., Prigent, C., Buchwitz, M., Schneising, O., Burrows, J. P., Wilson, C., Richards, N., Chipperfield, M., Comparison of the HadGEM2 climate-chemistry model against in-situ and SCIAMACHY atmospheric methane data, *Atmos. Chem. Phys.*, 14, 13257-13280, doi:10.5194/acp-14-13257-2014, 2014.

Hedelius, J. K., Parker, H., Wunch, D., Roehl, C. M., Viatte, C., Newman, S., Toon, G. C., Podolske, J. R., Hillyard, P. W., 650 Iraci, L. T., Dubey, M. K., and Wennberg, P. O.: Intercomparability of XCO<sub>2</sub> and XCH<sub>4</sub> from the United States TCCON sites, *Atmos. Meas. Tech.*, 10, 1481-1493, <https://doi.org/10.5194/amt-10-1481-2017>, 2017.



- Heymann, J., Reuter, M., Hilker, M., Buchwitz, M., Schneising, O., Bovensmann, H., Burrows, J. P., Kuze, A., Suto, H.,  
Deutscher, N. M., Dubey, M. K., Griffith, D. W. T., Hase, F., Kawakami, S., Kivi, R., Morino, I., Petri, C., Roehl, C.,  
Schneider, M., Sherlock, V., Sussmann, R., Velazco, V. A., Warneke, T., and Wunch, D.: Consistent satellite XCO<sub>2</sub>  
655 retrievals from SCIAMACHY and GOSAT using the BESD algorithm, *Atmos. Meas. Tech.*, 8, 2961–2980, 2015.
- Hollmann, R., Merchant, C. J., Saunders, R., Downy, C., Buchwitz, M., Cazenave, A., Chuvieco, E., Defourny, P., de  
Leeuw, G., Forsberg, R., Holzer-Popp, T., Paul, F., Sandven, S., Sathyendranath, S., van Roozendaal, M., and Wagner, W.:  
The ESA Climate Change Initiative: satellite data records for essential climate variables, *Bulletin of the American  
Meteorological Society (BAMS)*, 0.1175/BAMS-D-11-00254.1, 2013.
- 660 Howarth, R. W.: Ideas and perspectives: is shale gas a major driver of recent increase in global atmospheric methane?,  
*Biogeosciences*, 16, 3033–3046, <https://doi.org/10.5194/bg-16-3033-2019>, 2019.
- Houweling, S., Baker, D., Basu, S., Boesch, H., Butz, A., Chevallier, F., Deng, F., Dlugokencky, E. J., Feng, L., Ganshin,  
A., Hasekamp, O., Jones, D., Maksyutov, S., Marshall, J., Oda, T., O'Dell, C. W., Oshchepkov, S., Palmer, P. I., Peylin, P.,  
Poussi, Z., Reum, F., Takagi, H., Yoshida, Y., and Zhuravlev, R.: An intercomparison of inverse models for estimating  
665 sources and sinks of CO<sub>2</sub> using GOSAT measurements, *J. Geophys. Res. Atmos.*, 120, 5253–5266,  
[doi:10.1002/2014JD022962](https://doi.org/10.1002/2014JD022962), 2015.
- Hu, H., Landgraf, J., Detmers, R., Borsdorff, T., Aan de Brugh, J., Aben, I., Butz, A., and Hasekamp, O.: Toward Global  
Mapping of Methane With TROPOMI: First Results and Intersatellite Comparison to GOSAT, *Geophysical Research  
Letters*, 45, 3682–3689, <https://doi.org/10.1002/2018GL077259>, 2018.
- 670 IPCC: Climate Change 2013: The Physical Science Basis, Working Group I Contribution to the Fifth Assessment Report of  
the Intergovernmental Report on Climate Change, <http://www.ipcc.ch/report/ar5/wg1/> (last access: 21-February-2019),  
Cambridge University Press, 2013.
- Iraci, L., Podolske, J., Hillyard, P., Roehl, C., Wennberg, P. O., Blavier, J.-F., Landeros, J., Allen, N., Wunch, D., Zavaleta,  
J., Quigley, E., Osterman, G., Albertson, R., Dunwoody, K., and Boyden, H.: TCCON data from Edwards (US), Release  
675 GGG2014.R1. TCCON data archive, hosted by CaltechDATA,  
<https://doi.org/10.14291/tcon.ggg2014.edwards01.R1/1255068>, 2014.
- Kaminski, T., Scholze, M., Voßbeck, M., Knorr, W., Buchwitz, M., and Reuter, M.: Constraining a terrestrial biosphere  
model with remotely sensed atmospheric carbon dioxide, *Remote Sensing of Environment* 203, 109–124, 2017.
- Kivi, R. and Heikkinen, P.: Fourier transform spectrometer measurements of column CO<sub>2</sub> at Sodankylä, Finland, *Geosci.  
680 Instrum. Method. Data Syst.*, 5, 271–279, <https://doi.org/10.5194/gi-5-271-2016>, 2016.
- Kivi, R., Heikkinen, P., and Kyrö, E.: TCCON data from Sodankylä (FI), Release GGG2014R0. TCCON data archive,  
hosted by CaltechDATA, <https://doi.org/10.14291/tcon.ggg2014.sodankyla01.R0/1149280>, 2014.



- 685 Kuze, A., Suto, H., Shiomi, K., Kawakami, S., Tanaka, M., Ueda, Y., Deguchi, A., Yoshida, J., Yamamoto, Y., Kataoka, F., Taylor, T. E., and Buijs, H. L.: Update on GOSAT TANSO-FTS performance, operations, and data products after more than 6 years in space, *Atmos. Meas. Tech.*, 9, 2445-2461, doi:10.5194/amt-9-2445-2016, 2016.
- Lauer, A., Eyring, V., Righi, M., Buchwitz, M., Defourny, P., Evaldsson, M., Friedlingstein, P., de Jeu, R., de Leeuw, G., Loew, A., Merchant, C. J., Müller, B., Popp, T., Reuter, M., Sandven, S., Senfleben, D., Stengel, M., Van Roozendaal, M., Wenzel, S., and Willén, U.: Benchmarking CMIP5 models with a subset of ESA CCI Phase 2 data using the ESMValTool, *Remote Sensing of Environment*, 203, 9-39, <http://dx.doi.org/10.1016/j.rse.2017.01.007>, 2017.
- 690 Le Quéré, C., Andrew, R. M., Friedlingstein, P., Sitch, S., Pongratz, J., Manning, A. C., Korsbakken, J. I., Peters, G. P., Canadell, J. G., Jackson, R. B., Boden, T. A., Tans, P. P., Andrews, O. D., Arora, V. K., Bakker, D. D. E, Barbero, L., Becker, M., Betts, R. A., Bopp, L., Chevallier, F., Chini, L. P., Ciais, P., Cosca, C. E., Cross, J., Currie, K., Gasser, T., Harris, I., Hauck, J., Haverd, V., Houghton, R. A., Hunt, C. W., Hurtt, G., Ilyina, T., Jain, A. K., Kato, E., Kautz, M., Keeling, R. F., Goldewijk, K. K., Körtzinger, A., Landschützer, P., Lefèvre, N., Lenton, A., Lienert, S., Lima, I.,
- 695 Lombardozzi, D., Metzl, N., Millero, F., Monteiro, P. M. S., Munro, D. R., Nabel, J. E. M. S., Nakaoka, S., Nojiri, Y., Padín, X. A., Peregon, A., Pfeil, B., Pierrot, D., Poulter, B., Rehder, G., Reimer, J., Rödenbeck, C., Schwinger, J., Séférian, R., Skjelvan, I., Stocker, B. D., Tian, H., Tilbrook, B., van der Laan-Luijkx, I. T., van der Werf, G. R., van Heuven, S., Viovy, N., Vuichard, N., Walker, A. P., Watson, A. J., Wiltshire, A. J., Zaehle, S., and Zhu, D.: Global Carbon Budget 2017, *Earth System Science Data*, 10, 405-448, DOI: 10.5194/essd-10-405-2018, 2018.
- 700 Liu, J., Bowman, K. W., Schimel, D. S., Parazoo, N. C., Jiang, Z., Lee, M., Bloom, A. A., Wunch, D., Frankenberg, C., Sun, Y., O'Dell, C. W., Gurney, K. R., Menemenlis, D., Gierach, M., Crisp, D., and Eldering, A.: Contrasting carbon cycle responses of the tropical continents to the 2015–2016 El Niño, *Science*, 358, eaam5690, pp. 7, 2017.
- Maasackers, J. D., Jacob, D. J., Sulprizio, M. P., Scarpelli, T. R., Nesser, H., Sheng, J.-X., Zhang, Y., Hersher, M., Bloom, A. A., Bowman, K. W., Worden, J. R., Janssens-Maenhout, G., and Parker, R. J.: Global distribution of methane emissions, emission trends, and OH concentrations and trends inferred from an inversion of GOSAT satellite data for 2010–2015, *Atmos. Chem. Phys.*, 19, 7859–7881, <https://doi.org/10.5194/acp-19-7859-2019>, 2019.
- Morino, I., Matsuzaki, T., and Shishime, A.: TCCON data from Tsukuba, Ibaraki (JP) , 125HR, Release GGG2014R2. TCCON data archive, hosted by CaltechDATA, <https://doi.org/10.14291/tcon.ggg2014.tsukuba02.R2>, 2018a.
- Morino, I., Velasco, V. A., Hori, A., Uchino, O., and Griffith, D. W. T.: TCCON data from Burgos, Ilocos Norte (PH),  
710 Release GGG2014.R0. TCCON data archive, hosted by CaltechDATA,  
<https://doi.org/10.14291/tcon.ggg2014.burgos01.R0>, 2018b.



- Nassar, R., Hill, T. G., McLinden, C. A., Wunch, D., Jones, D. B. A., and Crisp, D.: Quantifying CO<sub>2</sub> emissions from individual power plants from space. *Geophysical Research Letters*, 44, 10,045–10,053.  
<https://doi.org/10.1002/2017GL074702>, 2017.
- 715 Nisbet, E. G., Manning, M. R., Dlugokencky, E. J., Fisher, R. E., Lowry, D., Michel, S. E., Lund Myhre, C., Platt, S. M., Allen, G., Bousquet, P., Brownlow, R., Cain, M., France, J. L., Hermansen, O., Hossaini, R., Jones, A. E., Levin, I., Manning, A. C., Myhre, G., Pyle, J. A., Vaughn, B., Warwick, N. J., and White, J. W. C.: Very strong atmospheric methane growth in the four years 2014-2017: Implications for the Paris Agreement. *Global Biogeochemical Cycles*, 33.  
<https://doi.org/10.1029/2018GB006009>, 2019.
- 720 Miller, S. M., Michalak, A. M., Detmers, R. G., Hasekamp, O. P., Bruhwiler, L. M. P., and Schwietzke, S.: China's coal mine methane regulations have not curbed growing emissions, *Nature Communications*, volume 10, article number: 303, 2019.
- Notholt, J., Schrems, O., Warneke, T., Deutscher, N. M., Weinzierl, C., Palm, M., and Buschmann, M.: TCCON data from Ny-Ålesund, Spitzbergen (NO), Release GGG2014R1. TCCON data archive, hosted by CaltechDATA,  
725 <https://doi.org/10.14291/tcon.ggg2014.nyalesund01.R1>, 2019a.
- Notholt, J., Petri, C., Warneke, T., Deutscher, N., Buschmann, M., Weinzierl, C., Macatangay, R., and Gruppe, P.: TCCON data from Bremen (DE), Release GGG2014R1. TCCON data archive, hosted by CaltechDATA,  
<https://doi.org/10.14291/tcon.ggg2014.bremen01.R1>, 2019b.
- O'Dell, C. W., Connor, B., Bösch, H., O'Brien, D., Frankenberg, C., Castano, R., Christi, M., Eldering, D., Fisher, B.,  
730 Gunson, M., McDuffie, J., Miller, C. E., Natraj, V., Oyafuso, F., Polonsky, I., Smyth, M., Taylor, T., Toon, G. C., Wennberg, P. O., and Wunch, D.: The ACOS CO<sub>2</sub> retrieval algorithm – Part 1: The ACOS CO<sub>2</sub> retrieval algorithm – Part 1: Description and validation against synthetic observations, *Atmos. Meas. Tech.*, 5, 99–121, doi:10.5194/amt-5-99-2012, 2012.
- O'Dell, C. W., Eldering, A., Wennberg, P. O., Crisp, D., Gunson, M. R., Fisher, B., Frankenberg, C., Kiel, M., Lindqvist, H., Mandrake, L., Merrelli, A., Natraj, V., Nelson, R. R., Osterman, G. B., Payne, V. H., Taylor, T. R., Wunch, D., Drouin, B. J.,  
735 Oyafuso, F., Chang, A., McDuffie, J., Smyth, M., Baker, D. F., Basu, S., Chevallier, F., Crowell, S. M. R., Feng, L., Palmer, P. I., Dubey, M., García, O. E., 15 Griffith, D. W. T., Hase, F., Iraci, L. T., Kivi, R., Morino, I., Notholt, J., Ohyama, H., Petri, C., Roehl, C. M., Sha, M. K., Strong, K., Sussmann, R., Te, Y., Uchino, O., and Velasco, V. A.: Improved Retrievals of Carbon Dioxide from the Orbiting Carbon Observatory-2 with the version 8 ACOS algorithm, *Atmospheric Measurement Techniques*, *Atmos. Meas. Tech.*, 11, 6539-6576, <https://doi.org/10.5194/amt-11-6539-2018>, 2018.
- 740 Parker, R., Boesch, H., Cogan, A., Fraser, A., Feng, L., Palmer, P., Messerschmidt, J., Deutscher, N., Griffith, D., Notholt, J., Wennberg, and P. Wunch, D.: Methane Observations from the Greenhouse gases Observing SATellite: Comparison to ground-based TCCON data and Model Calculations, *Geophys. Res. Lett.*, doi:10.1029/2011GL047871, 2011.



- Peters, W., Jacobson, A. R., Sweeney, C., Andrews, A. E., Con-way, T. J., Masarie, K., Miller, J. B., Bruhwiler, L. M. P., Pétron, G., Hirsch, A. I., Worthy, D. E. J., van der Werf, G. R., Randerson, J. T., Wennberg, P. O., Krol, M. C., and Tans, P. P.: An atmospheric perspective on North American carbon dioxide exchange: CarbonTracker, Proceedings of the National Academy of Sciences (PNAS) of the United States of America, 104,18925–18930,doi:10.1073/pnas.0708986104, 2007.
- 745 Reuter, M., Buchwitz, M., Schneising, O., Heymann, J., Bovensmann, H., and Burrows, J. P.: A method for improved SCIAMACHY CO<sub>2</sub> retrieval in the presence of optically thin clouds, Atmos. Meas. Tech., 3, 209-232, 2010.
- Reuter, M., Bovensmann, H., Buchwitz, M., Burrows, J. P., Connor, B. J., Deutscher, N. M., Griffith, D. W. T., Heymann, J., Keppel-Aleks, G., Messerschmidt, J., Notholt, J., Petri, C., Robinson, J., Schneising, O., Sherlock, V., Velasco, V., Warneke, W., Wennberg, P. O., and Wunch, D.: Retrieval of atmospheric CO<sub>2</sub> with enhanced accuracy and precision from SCIAMACHY: Validation with FTS measurements and comparison with model results, J. Geophys. Res., 116, D04301, doi:10.1029/2010JD015047, 2011.
- 750 Reuter, M., Buchwitz, M., Schneising, O., Hase, F., Heymann, J., Guerlet, S., Cogan, A. J., Bovensmann, H., and Burrows, J. P.: A simple empirical model estimating atmospheric CO<sub>2</sub> background concentrations, Atmos. Meas. Tech., 5, 1349-1357, 2012.
- 755 Reuter, M., Boesch, H., Bovensmann, H., Bril, A., Buchwitz, M., Butz, A., Burrows, J. P., O'Dell, C. W., Guerlet, S., Hasekamp, O., Heymann, J., Kikuchi, N., Oshchepkov, S., Parker, R., Pfeifer, S., Schneising, O., Yokota, T., and Yoshida, Y.: A joint effort to deliver satellite retrieved atmospheric CO<sub>2</sub> concentrations for surface flux inversions: the ensemble median algorithm EMMA, Atmos. Chem. Phys., 13, 1771-1780, 2013.
- 760 Reuter, M., Buchwitz, M., Hilker, M., Heymann, J., Schneising, O., Pillai, D., Bovensmann, H., Burrows, J. P., Bösch, H., Parker, R., Butz, A., Hasekamp, O., O'Dell, C. W., Yoshida, Y., Gerbig, C., Nehr Korn, T., Deutscher, N. M., Warneke, T., Notholt, J., Hase, F., Kivi, R., Sussmann, R., Machida, T., Matsueda, H., and Sawa, Y.: Satellite-inferred European carbon sink larger than expected, Atmos. Chem. Phys., 14, 13739-13753, 2014a.
- 765 Reuter, M., Buchwitz, M., Hilboll, A., Richter, A., Schneising, O., Hilker, M., Heymann, J., Bovensmann, H., and Burrows, J. P.: Decreasing emissions of NO<sub>x</sub> relative to CO<sub>2</sub> in East Asia inferred from satellite observations, Nature Geoscience, 28 Sept. 2014, doi:10.1038/ngeo2257, pp. 4, 2014b.
- 770 Reuter, M., Buchwitz, M., Schneising, O., Noël, S., Rozanov, V., Bovensmann, H., and Burrows, J. P.: A Fast Atmospheric Trace Gas Retrieval for Hyperspectral Instruments Approximating Multiple Scattering - Part 1: Radiative Transfer and a Potential OCO-2 XCO<sub>2</sub> Retrieval Setup, Remote Sens., 9, 1159, doi:10.3390/rs9111159, 2017a.
- Reuter, M., Buchwitz, M., Schneising, O., Noël, S., Bovensmann, H., and Burrows, J. P.: A Fast Atmospheric Trace Gas Retrieval for Hyperspectral Instruments Approximating Multiple Scattering - Part 2: Application to XCO<sub>2</sub> Retrievals from OCO-2, Remote Sens., 9, 1102, doi:10.3390/rs9111102, 2017b.



- Reuter, M., Buchwitz, M., Schneising, O., Krautwurst, S., O'Dell, C. W., Richter, A., Bovensmann, H., and Burrows, J. P.:  
775 Towards monitoring localized CO<sub>2</sub> emissions from space: co-located regional CO<sub>2</sub> and NO<sub>2</sub> enhancements observed by the  
OCO-2 and S5P satellites, *Atmos. Chem. Phys.*, <https://www.atmos-chem-phys.net/19/9371/2019/>, 19, 9371-9383, 2019a.
- Reuter, M., Buchwitz, M., and Schneising-Weigel, O.: Algorithm Theoretical Basis Document (ATBD) – ANNEX D for  
products XCO<sub>2</sub>\_EMMA, XCH<sub>4</sub>\_EMMA, XCO<sub>2</sub>\_OBS4MIPS, XCH<sub>4</sub>\_OBS4MIPS (v4.1, 2003-2018), Technical Report  
Copernicus Climate Change Service (C3S), version 3.0, 12-08-2019, pp. 35, access: available in December 2019 from CDS  
780 website (<https://cds.climate.copernicus.eu>), 2019b.
- Reuter, M., Buchwitz, M., and Schneising-Weigel, O.: Product Quality Assessment Report (PQAR) – ANNEX D for  
products XCO<sub>2</sub>\_EMMA, XCH<sub>4</sub>\_EMMA, XCO<sub>2</sub>\_OBS4MIPS, XCH<sub>4</sub>\_OBS4MIPS (v4.1, 2003-2018), Technical Report  
Copernicus Climate Change Service (C3S), version 3.0, 12-08-2019, pp. 36, access: available in December 2019 from CDS  
website (<https://cds.climate.copernicus.eu>), 2019c.
- 785 Reuter, M., Buchwitz, M., and Schneising-Weigel, O.: Product User Guide and Specification (PUGS) – ANNEX D for  
products XCO<sub>2</sub>\_EMMA, XCH<sub>4</sub>\_EMMA, XCO<sub>2</sub>\_OBS4MIPS, XCH<sub>4</sub>\_OBS4MIPS (v4.1, 2003-2018), Technical Report  
Copernicus Climate Change Service (C3S), version 3.0, 12-08-2019, pp. 22, access: available in December 2019 from CDS  
website (<https://cds.climate.copernicus.eu>), 2019d.
- Rodgers, C. D., *Inverse Methods for Atmospheric Sounding: Theory and Practice*, World Scientific Publishing, 2000.
- 790 Schaefer, H.: On the Causes and Consequences of Recent Trends in Atmospheric Methane, *Curr. Clim. Change Rep.*,  
<https://doi.org/10.1007/s40641-019-00140-z>, 2019.
- Sheng, J.-X., Jacob, D. J., Turner, A. J., Maasakkers, J. D., Benmergui, J., Bloom, A. A., Arndt, C., Gautam, R., Zavala-  
Araiza, D., Boesch, H., and Parker, R. J.: 2010–2016 methane trends over Canada, the United States, and Mexico observed  
by the GOSAT satellite: contributions from different source sectors, *Atmos. Chem. Phys.*, 18, 12257–12267,  
795 <https://doi.org/10.5194/acp-18-12257-2018>, 2018.
- Schneising, O., Buchwitz, M., Reuter, M., Heymann, J., Bovensmann, H., and Burrows, J. P.: Long-term analysis of carbon  
dioxide and methane column-averaged mole fractions retrieved from SCIAMACHY, *Atmos. Chem. Phys.*, 11, 2881-2892,  
2011.
- Schneising, O., Reuter, M., Buchwitz, M., Heymann, J., Bovensmann, H., and Burrows, J. P.: Terrestrial carbon sink  
800 observed from space: variation of growth rates and seasonal cycle amplitudes in response to interannual surface temperature  
variability, *Atmos. Chem. Phys.*, 14, 133-141, 2014a.
- Schneising, O., Burrows, J. P., Dickerson, R. R., Buchwitz, M., Reuter, M., and Bovensmann, H.: Remote sensing of  
fugitive methane emissions from oil and gas production in North American tight geologic formations, *Earth's Future*, 2, doi:  
10.1002/2014EF000265, pp. 11, 2014b.





- 805 Schneising, O., Buchwitz, M., Reuter, M., Bovensmann, H., Burrows, J. P., Borsdorff, T., Deutscher, N. M., Feist, D. G., Griffith, D. W. T., Hase, F., Hermans, C., Iraci, L. T., Kivi, R., Landgraf, J., Morino, I., Notholt, J., Petri, C., Pollard, D. F., Roche, S., Shiomi, K., Strong, K., Sussmann, R., Velazco, V. A., Warneke, T., and Wunch, D.: A scientific algorithm to simultaneously retrieve carbon monoxide and methane from TROPOMI onboard Sentinel-5 Precursor, *Atmos. Meas. Tech. Discuss.*, <https://www.atmos-meas-tech-discuss.net/amt-2019-243/>, in review, 2019.
- 810 Sherlock, V., Connor, B., Robinson, J., Shiona, H., Smale, D., and Pollard, D. F.: TCCON data from Lauder (NZ), 125HR, Release GGG2014R0. TCCON data archive, hosted by CaltechDATA, <https://doi.org/10.14291/tccon.ggg2014.lauder02.R0/1149298>, 2014.
- Shiomi, K., Kawakami, S., Ohyama, H., Arai, K., Okumura, H., Taura, C., Fukamachi, T., and Sakashita, M.: TCCON data from Saga (JP), Release GGG2014R0. TCCON data archive, hosted by CaltechDATA,
- 815 <https://doi.org/10.14291/tccon.ggg2014.saga01.R0/1149283>, 2014.
- Strong, K., Roche, S., Franklin, J. E., Mendonca, J., Lutsch, E., Weaver, D., Fogal, P. F., Drummond, J. R., Batchelor, R., and Lindenmaier, R.: TCCON data from Eureka (CA), Release GGG2014R3. TCCON data archive, hosted by CaltechDATA, <https://doi.org/10.14291/tccon.ggg2014.eureka01.R3>, 2019.
- Sussmann, R. and Rettinger, M.: TCCON data from Garmisch (DE), Release GGG2014R2. TCCON data archive, hosted by
- 820 Caltech-DATA, <https://doi.org/10.14291/tccon.ggg2014.garmisch01.R2>, 2018.
- Té, Y., Jeseck, P. and Janssen, C.: TCCON data from Paris (FR), Release GGG2014R0. TCCON data archive, hosted by CaltechDATA, <https://doi.org/10.14291/tccon.ggg2014.paris01.R0/1149279>, 2014.
- Turner, A. J., Jacob, D. J., Wecht, K. J., Maasakkers, J. D., Biraud, S. C., Boesch, H., Bowman, K. W., Deutscher, N. M., Dubey, M. K., Griffith, D. W. T., Hase, F., Kuze, A., Notholt, J., Ohyama, H., Parker, R., Payne, V. H., Sussmann, R.,
- 825 Velazco, V. A., Warneke, T., Wennberg, P. O., and Wunch, D.: Estimating global and North American methane emissions with high spatial resolution using GOSAT satellite data, *Atmos. Chem. Phys.*, 15, 7049-7069, doi:10.5194/acp-15-7049-2015, 2015.
- Turner, A. J., Frankenberg, C., and Kort, E. A.: Interpreting contemporary trends in atmospheric methane, *Proceedings of the National Academy of Sciences*, 116 (8), 2805-2813; DOI: 10.1073/pnas.1814297116, 2019.
- 830 Veefkind, J. P., Aben, I., McMullan, K., Förster, H., De Vries, J., Otter, G., Claas, J., Eskes, H. J., De Haan, J. F., Kleipool, Q., Van Weele, M., Hasekamp, O., Hoogeveen, R., Landgraf, J., Snel, R., Tol, P., Ingmann, P., Voors, R., Kruizinga, B., Vink, R., Visser, H., and Levelt, P. F.: TROPOMI on the ESA Sentinel-5 Precursor: A GMES mission for global observations of the atmospheric composition for climate, air quality and ozone layer applications. *Rem. Sens. Environment*, 120:70–83, 2012.



- 835 Velazco V. A., Morino, I., Uchino, O., Hori, A., Kiel, M., Bukosa, B., Deutscher, N. M., Sakai, T., Nagai, T., Bagtasa, G., Izumi, T., Yoshida, Y., and, Griffith, D. W. T.: TCCON Philippines: First Measurement Results, Satellite Data and Model Comparisons in Southeast Asia, *Remote Sens.*, 9(12),1228, <https://doi.org/10.3390/rs9121228>, 2017.
- Warneke, T., Messerschmidt, J., Notholt, J., Weinzierl, 5 C., Deutscher, N. M., Petri, C., Grupe, P., Vuillemin, C., Truong, F., Schmidt, M., Ramonet, M., and Parmentier, E.: TCCON data from Orléans (FR), Release GGG2014R1. TCCON data  
840 archive, hosted by CaltechDATA, <https://doi.org/10.14291/tcon.ggg2014.orleans01.R1>, 2019.
- Wennberg, P. O., Wunch, D., Roehl, C. M., Blavier, J.-F., Toon, G. C., and Allen, N. T.: TCCON data from Caltech (US), Release GGG2014R1. TCCON data archive, hosted by CaltechDATA, <https://doi.org/10.14291/tcon.ggg2014.pasadena01.R1/1182415>, 2015.
- Wennberg, P. O., Wunch, D., Roehl, C. M., Blavier, J.-F., Toon, G. C., Allen, N. T., Dowell, P., Teske, K., Martin, C., and  
845 Martin, J.: TCCON data from Lamont (US), Release GGG2014R1. TCCON data archive, hosted by CaltechDATA, <https://doi.org/10.14291/tcon.ggg2014.lamont01.R1/1255070>, 2016.
- Wennberg, P. O., Roehl, C. M., Wunch, D., Toon, G. C., Blavier, J.-F., Washenfelder, R., Keppel-Aleks, G., Allen, N. T., and Ayers, J.: TCCON data from Park Falls (US), Release GGG2014R1. TCCON data archive, hosted by CaltechDATA, <https://doi.org/10.14291/tcon.ggg2014.parkfalls01.R1>, 2017.
- 850 Worden, J. R., Bloom, A. A., Pandey, S., Jiang, Z., Worden, H. M., Walter, T. W., Houweling, S., and Röckmann, T.: Reduced biomass burning emissions reconcile conflicting estimates of the post-2006 atmospheric methane budget, *Nat. Commun.*, 8, 2227, <https://doi.org/10.1038/s41467-017-02246-0>, 2017.
- Wu, L., Hasekamp, O., Hu, H., Landgraf, J., Butz, A., aan de Brugh, J., Aben, I., Pollard, D. F., Griffith, D. W. T., Feist, D. G., Koshelev, D., Hase, F., Toon, G. C., Ohyama, H., Morino, I., Notholt, J., Shiomi, K., Iraci, L., Schneider, M., de  
855 Mazière, M., Sussmann, R., Kivi, R., Warneke, T., Goo, T.-Y., and Té, Y.: Carbon dioxide retrieval from OCO-2 satellite observations using the RemoTeC algorithm and validation with TCCON measurements, *Atmos. Meas. Tech.*, 11, 3111–3130, <https://doi.org/10.5194/amt-11-3111-2018>, 2018.
- Wu, L., Aben, I., Hasekamp, O. P., and Buchwitz, M.: Product Quality Assessment Report (PQAR) – ANNEX B for products CO<sub>2</sub>\_GOS\_SRFP, CH<sub>4</sub>\_GOS\_SRFP (v2.3.8, 2009-2018), Technical Report Copernicus Climate Change Service  
860 (C3S), version 3.0, 12-08-2019, pp. 36, access: available in December 2019 from CDS website (<https://cds.climate.copernicus.eu>), 2019.
- Wunch, D., Toon, G.C., Wennberg, P.O., Wofsy, S.C., Stephens, B.B., Fischer, M.L., Uchino, O., Abshire, J.B., Bernath, P., Biraud, S.C., Blavier, J.-F.L., Boone, C., Bowman, K.P., Browell, E.V., Campos, T., Connor, B.J., Daube, B.C., Deutscher, N.M., Diao, M., Elkins, J.W., Gerbig, C., Gottlieb, E., Griffith, D.W.T., Hurst, D.F., Jimenez, R., Keppel-Aleks, G., Kort,  
865 E.A., Macatangay, R., Machida, T., Matsueda, H., Moore, F., Morino, I., Park, S., Robinson, J., Roehl, C.M., Sawa, Y.,



- Sherlock, V., Sweeney, C., Tanaka, T., Zondlo, M.A.: Calibration of the total carbon column observing network using aircraft profile data. *Atmos. Meas. Tech.* 3:1351–1362. <http://dx.doi.org/10.5194/amt-3-1351-2010>, 2010.
- Wunch, D., Toon, G. C., Blavier, J.-F. L., Washenfelder, R. A., Notholt, J., Connor, B. J., Griffith, D. W. T., Sherlock, V., and Wennberg, P. O.: The Total Carbon Column Observing Network. *Phil. Trans. R. Soc. A*, 369, 2087–2112, doi:10.1098/rsta.2010.0240, 2011.
- 870
- Wunch, D., Mendonca, J., Colebatch, O., Allen, N. T., Blavier, J.-F., Roche, S., Hedelius, J., Neufeld, G., Springett, S., Worthy, D., Kessler, R., and Strong, K.: TCCON data from East Trout Lake, SK (CA), Release GGG2014.R1. TCCON data archive, hosted by CaltechDATA, <https://doi.org/10.14291/tcon.ggg2014.easttroutlake01.R1>, 2018.
- Yin, Y., Ciais, P., Chevallier, F., Li, W., Bastos, A., Piao, S., Wang, T., and Liu, H.: Changes in the response of the Northern Hemisphere carbon uptake to temperature over the last three decades. *Geophysical Research Letters*, 45, 4371–4380, <https://doi.org/10.1029/2018GL077316>, 2018.
- 875
- Yoshida, Y., Kikuchi, N., Morino, I., Uchino, O., Oshchepkov, S., Bril, A., Saeki, T., Schutgens, N., Toon, G. C., Wunch, D., Roehl, C. M., Wennberg, P. O., Griffith, D. W. T., Deutscher, N. M., Warneke, T., Notholt, J., Robinson, J., Sherlock, V., Connor, B., Rettinger, M., Sussmann, R., Ahonen, P., Heikkinen, P., Kyrö, E., Mendonca, J., Strong, K., Hase, F., Dohe, S., and Yokota, T.: Improvement of the retrieval algorithm for GOSAT SWIR XCO<sub>2</sub> and XCH<sub>4</sub> and their validation using TCCON data, *Atmos. Meas. Tech.*, 6, 1533–1547, doi:10.5194/amt-6-1533-2013, 2013.
- 880



**Tables:**

890 **Table 1. Satellite XCO<sub>2</sub> Level 2 (L2) data products used as input for the generation of the merged L2 and L3 XCO<sub>2</sub> version 4.1 data products. For products which have been generated in the framework of the CCI and C3S projects the corresponding product ID is listed (the other products are “external products”, which have been obtained from the corresponding websites (see Acknowledgements)). Temporal coverage indicates the time coverage of the input data sets.**

Algorithm / product acronym	Algorithm / product version	CCI / C3S product ID	Satellite / sensor	Temporal coverage	Comment	Reference
BESD	v02.01.02	CO2_SCI_BESD	SCIAMACHY	01/2003-03/2012	-	Reuter et al., 2011
UoL-FP	v7.2	CO2_GOS_OCFP	GOSAT	04/2009-12/2018	-	Cogan et al., 2012
RemoTeC	v2.3.8	CO2_GOS_SRFP	GOSAT	04/2009-12/2018	-	Butz et al., 2011
NIES	v02.75bc	-	GOSAT	04/2009 – 11/2018	Bias corrected operational NIES algorithm	Yoshida et al., 2013
PPDF-S	v02	-	GOSAT	06/2009 – 07/2015	-	Bril et al., 2012
ACOS	v7.3.10a	-	GOSAT	04/2009 – 05/2016	NASA ACOS GOSAT algorithm	O’Dell et al., 2012
ACOS	v9.0.03	-	OCO-2	09/2014 – 12/2018	NASA operational OCO-2 algorithm	O’Dell et al., 2018
FOCAL	v08	-	OCO-2	01/2015 - 12/2018	-	Reuter et al., 2017a, 2017b



895 Table 2. As Tab. 1 but for XCH<sub>4</sub>.

Algorithm / product acronym	Algorithm / product version	CCI / C3S product ID	Satellite / sensor	Temporal coverage	Comment	Reference
WFMD	v4.0	CH4_SCI_WFMD	SCIAMACHY	01/2003-12/2011	-	Schneising et al., 2011
UoL-FP	v7.2	CH4_GOS_OCFP	GOSAT	04/2009-12/2018	Univ. Leicester Full Physics (FP) algorithm	Parker et al., 2011
UoL-PR	v7.2	CH4_GOS_OCPR	GOSAT	04/2009-12/2018	Univ. Leicester Proxy (PR) algorithm	Parker et al., 2011
RemoTeC-FP	v2.3.8	CH4_GOS_SRFP	GOSAT	04/2009-12/2018	SRON Full Physics (FP) algorithm	Butz et al., 2011
RemoTeC-PR	v2.3.9	CH4_GOS_SRPR	GOSAT	04/2009-12/2018	SRON Proxy (PR) algorithm	Butz et al., 2010
NIES	v02.75bc	-	GOSAT	04/2009 – 11/2018	Bias corrected operational NIES algorithm	Yoshida et al., 2013
PPDF-S	v02	-	GOSAT	06/2009 – 07/2015	-	Bril et al., 2012



900 **Table 3. TCCON sites used for the validation of the XCO<sub>2</sub> and XCH<sub>4</sub> satellite-derived data products.**

<b>TCCON site (Acronym)</b>	<b>Latitude [deg]</b>	<b>Longitude [deg]</b>	<b>Altitude [km]</b>	<b>Start of time series</b>	<b>Reference</b>
Eureka, Canada (EUR)	80.05	-86.42	0.61	07.2010	Strong et al., 2019
Ny-Ålesund, Spitzbergen (NYL)	78.92	11.92	0.02	04.2014	Notholt et al., 2019a
Sodankylä, Finland (SOD)	67.37	26.63	0.19	05.2009	Kivi et al., 2014, 2016
East Trout Lake, Canada (ETL)	54.35	-104.99	0.50	10.2016	Wunch et al., 2018
Białystok, Poland (BIA)	53.23	23.03	0.19	03.2009	Deutscher et al., 2019
Bremen, Germany (BRE)	53.10	8.85	0.03	01.2010	Notholt et al., 2019b
Karlsruhe, Germany (KAR)	49.10	8.44	0.11	04.2010	Hase et al., 2015
Paris, France (PAR)	48.85	2.36	0.06	09.2014	Té et al., 2014
Orléans, France (ORL)	47.97	2.11	0.13	08.2009	Warneke et al., 2019
Garmisch, Germany (GAR)	47.48	11.06	0.75	07.2007	Sussmann and Rettinger, 2018
Park Falls, WI, USA (PFA)	45.94	-90.27	0.44	06.2004	Wennberg et al., 2017
Lamont, OK, USA (LAM)	36.60	-97.49	0.32	07.2008	Wennberg et al., 2016





Tsukuba, Japan (TSU)	36.05	140.12	0.03	08.2011	Morino et al., 2018a
Edwards, CA, USA (EDW)	34.96	-117.88	0.70	07.2013	Iraci et al., 2014
Caltech, CA, USA (CAL)	34.14	-118.13	0.24	09.2012	Wennberg et al., 2015
Saga, Japan (SAG)	33.24	130.29	0.01	07.2011	Shiomi et al., 2014
Burgos, Philippines (BUR)	18.53	120.65	0.04	03.2017	Morino et al., 2018b; Velazco et al., 2017
Ascension Island (ASC)	-7.92	-14.33	0.03	10.2018	Feist et al., 2014
Darwin, Australia (DAR)	-12.46	130.93	0.04	08.2005	Griffith et al., 2014b
Réunion Island (REU)	-20.90	55.49	0.09	09.2011	De Mazière et al., 2017
Wollongong, Australia (WOL)	-34.41	150.88	0.03	06.2008	Griffith et al., 2014a
Lauder, New Zealand (LAU)	-45.04	169.68	0.37	02.2010	Sherlock et al., 2014



**Table 4. Overview validation results at TCCON sites for data product XCO<sub>2</sub>\_EMMA (version 4.1).**

905

TCCON site	Random error sgObs. (1-sigma) [ppm]		Uncertainty ratio [-]		Overall bias satellite – TCCON [ppm]		Seasonal bias satellite – TCCON [ppm]	
	QA/QC	EMMA	QA/QC	EMMA	QA/QC	EMMA	QA/QC	EMMA
SOD	1.19	1.33	1.16	1.10	0.57	0.18	-	0.22
BIA	1.11	1.16	1.44	1.37	0.06	0.10	-	0.26
BRE	1.66	1.30	0.90	1.14	1.09	0.55	-	0.15
KAR	1.45	1.40	0.96	0.99	1.18	0.52	1.17	0.40
PAR	1.30	-	0.99	-	-0.49	-	-	-
ORL	1.18	1.40	1.15	1.04	0.30	0.45	0.75	0.39
GAR	1.48	1.46	0.91	1.04	1.28	0.36	0.83	0.22
PFA	1.08	1.27	1.31	1.11	0.09	-0.37	0.70	0.18
LAM	1.26	1.47	1.08	0.95	-0.09	-0.61	0.17	0.38
TSU	1.54	-	0.95	-	0.54	-	0.61	-
EDW	1.48	-	0.78	-	1.16	-	0.21	-
CAL	1.57	-	0.75	-	-0.46	-	0.15	-
SAG	1.41	-	1.06	-	-0.17	-	0.31	-
ASC	1.16	-	1.44	-	0.65	-	0.60	-
DAR	1.06	1.06	1.01	1.02	-0.23	0.52	0.66	0.34
REU	0.75	-	1.73	-	0.29	-	-	-
WOL	1.21	1.19	1.00	1.00	-0.53	-0.66	0.24	0.17
LAU	1.13	-	1.03	-	0.14	-	0.10	-
<b>Mean</b>	<b>1.28</b>	<b>1.30</b>	<b>1.15</b>	<b>1.07</b>	<b>0.30</b>	<b>0.10</b>	<b>0.50</b>	<b>0.27</b>
<b>StdDev</b>	<b>0.23</b>	<b>0.14</b>	<b>0.23</b>	<b>0.12</b>	<b>0.60</b>	<b>0.48</b>	<b>0.33</b>	<b>0.10</b>



910 **Table 5. Validation summary for data product XCO<sub>2</sub>\_EMMA (version 4.1).**

Parameter	Assessment method		Mean
	QA/QC	EMMA	
Random error single observations (1-sigma) [ppm]	1.28	1.30	1.29
Global bias [ppm]	0.30	0.10	0.20
Regional bias (1-sigma) [ppm]	0.60	0.48	0.54
Seasonal bias (1-sigma) [ppm]	0.50	0.27	0.39
Spatio-temporal bias (1-sigma) [ppm]	0.78	0.55	0.66



915 **Table 6.** TCCON XCO<sub>2</sub> bias in ppm (satellite - TCCON). Assessment method DP is the method used by the data provider, for (\*) see Boesch et al., 2019, and for (#) see Wu et al., 2019. “-“ means that the number of available collocations is less than the threshold required by the corresponding assessment method. Note that this table includes only a subset of the 10 sites shown in in Fig. 11, namely only those sites with a mean bias being considerably (more than 1.5 times) larger than the standard deviation of the biases.

Satellite product	Assessment method	TCCON site			
		SOD	KAR	ORL	LAM
XCO2_EMMA	QA/QC	0.57	1.18	0.30	-0.09
	EMMA	0.18	0.52	0.45	-0.61
CO2_SCI_BESD	QA/QC	0.27	-	0.09	-0.27
	EMMA	0.32	0.39	0.25	-0.08
CO2_GOS_OCFP	QA/QC	0.32	0.83	0.33	-0.32
	EMMA	0.25	0.40	0.23	-0.61
	DP (*)	0.57	0.11	0.05	-0.33
CO2_GOS_SRFP	QA/QC	0.49	1.09	0.31	-0.59
	EMMA	0.61	0.49	0.20	-0.96
	DP (#)	0.89	0.49	0.49	-0.41
GOS NIES	EMMA	0.29	0.50	0.22	-0.78
GOS NASA	EMMA	1.04	0.14	0.03	-0.73
OCO-2 FOCAL	EMMA	0.02	0.18	0.29	-0.34
OCO-2 NASA	EMMA	0.40	0.29	0.36	-0.41
<b>Mean</b>		<b>0.44</b>	<b>0.51</b>	<b>0.26</b>	<b>-0.47</b>
<b>Standard deviation</b>		<b>0.28</b>	<b>0.34</b>	<b>0.14</b>	<b>0.26</b>

920



925 **Table 7. Overview validation results at TCCON sites for data product XCH4\_EMMA (version 4.1).**

TCCON site	Random error sgObs. (1-sigma) [ppb]		Uncertainty ratio [-]		Overall bias satellite – TCCON [ppb]		Seasonal bias satellite – TCCON [ppb]	
	QA/QC	EMMA	QA/QC	EMMA	QA/QC	EMMA	QA/QC	EMMA
SOD	14.2	14.9	1.11	1.05	2.2	4.5	-	1.6
ETL	15.2	-	0.98	-	3.0	-	-	-
BIA	17.6	13.6	0.91	0.99	-2.3	0.7	4.1	1.5
BRE	12.3	13.9	1.13	1.01	-2.1	-0.5	-	2.8
KAR	12.8	14.1	1.10	0.97	-5.3	1.4	1.3	1.7
PAR	11.3	-	1.13	-	-7.9	-	1.1	-
ORL	11.3	12.8	1.17	1.05	-3.0	0.8	1.0	1.5
GAR	39.0	14.2	0.74	1.04	0.2	1.7	1.8	3.3
PFA	61.7	13.9	0.92	1.01	-9.1	4.4	3.7	2.9
LAM	47.1	13.1	0.89	0.91	-0.6	-1.0	0.6	1.8
TSU	13.2	-	1.08	-	-1.3	-	2.7	-
EDW	15.9	-	0.82	-	1.8	-	3.0	-
CAL	15.9	-	0.82	-	-10.8	-	2.7	-
SAG	12.5	-	1.06	-	-2.7	-	1.9	-
ASC	10.1	-	1.07	-	-5.3	-	1.2	-
DAR	58.1	10.0	1.21	1.02	-18.2	-5.7	3.1	1.9
REU	9.8	-	0.99	-	-3.0	-	-	-
WOL	16.5	15.6	0.76	0.74	-8.8	-6.4	2.6	5.7
LAU	9.0	-	1.12	-	-3.1	-	1.7	-
<b>Mean</b>	<b>21.2</b>	<b>13.6</b>	<b>1.01</b>	<b>0.98</b>	<b>-4.0</b>	<b>0.0</b>	<b>2.2</b>	<b>2.5</b>
<b>StdDev</b>	<b>16.8</b>	<b>1.5</b>	<b>0.16</b>	<b>0.09</b>	<b>5.2</b>	<b>3.7</b>	<b>1.1</b>	<b>1.3</b>



930

**Table 8. Validation summary for data product XCH4\_EMMA (version 4.1).**

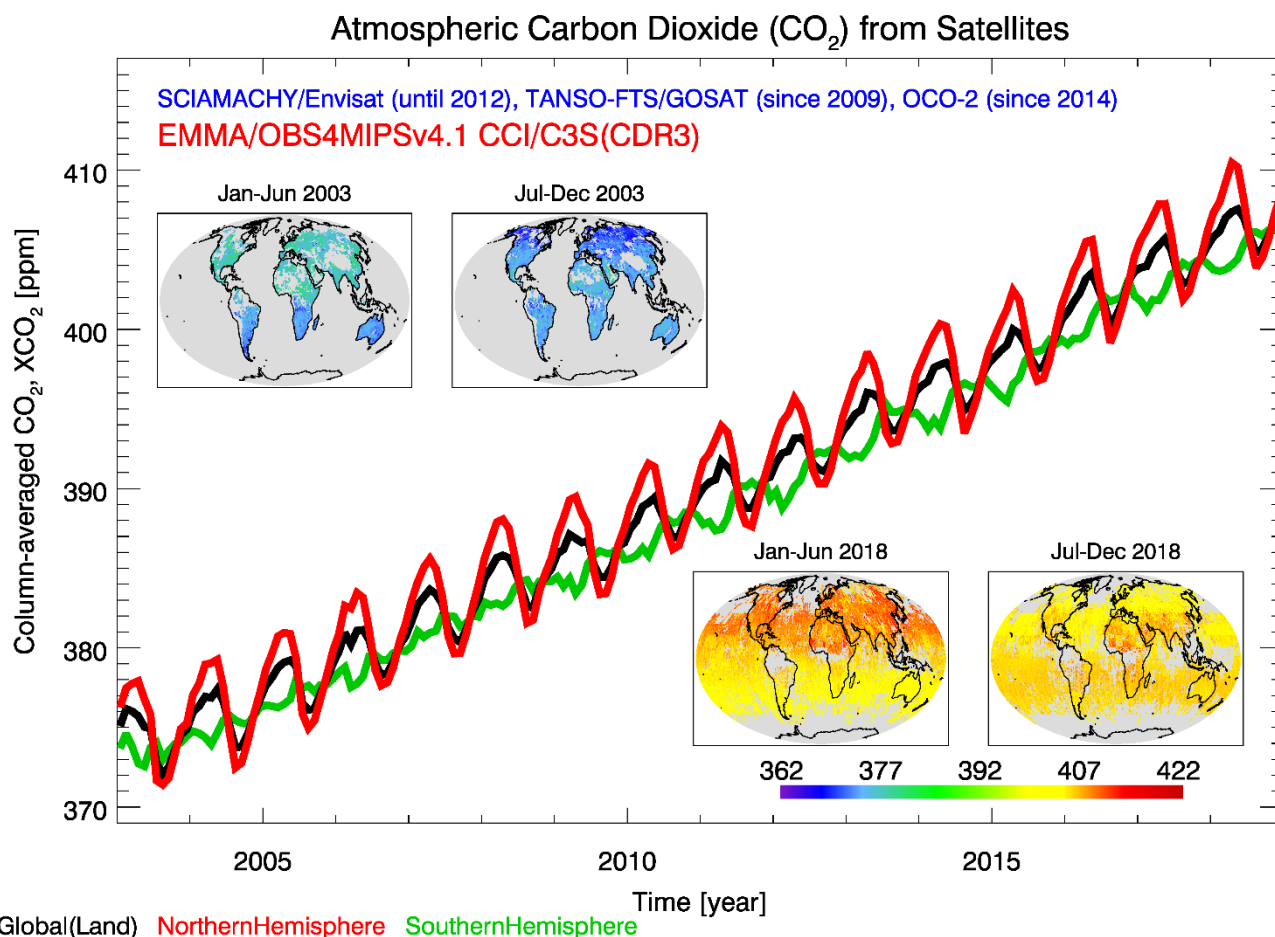
Parameter	Assessment method		Mean
	QA/QC	EMMA	
Random error single observations (1-sigma) [ppb]	21.2	13.6	17.4
Global bias [ppb]	-4.0	0.0	-2.0
Regional bias (1-sigma) [ppb]	5.2	3.7	4.4
Seasonal bias (1-sigma) [ppb]	2.2	2.5	2.3
Spatio-temporal bias (1-sigma) [ppb]	5.6	4.4	5.0





935

Figures:



940 **Figure 1:** Overview of the presented XCO<sub>2</sub> data set. Shown are time series over land for three latitude bands (global (black line), northern hemisphere (red), southern hemisphere (green)) and global maps (half-yearly averages at 1°x1° obtained by gridding (averaging) the merged Level 2, i.e., EMMA, product). See Sect. 4 for a detailed discussion.

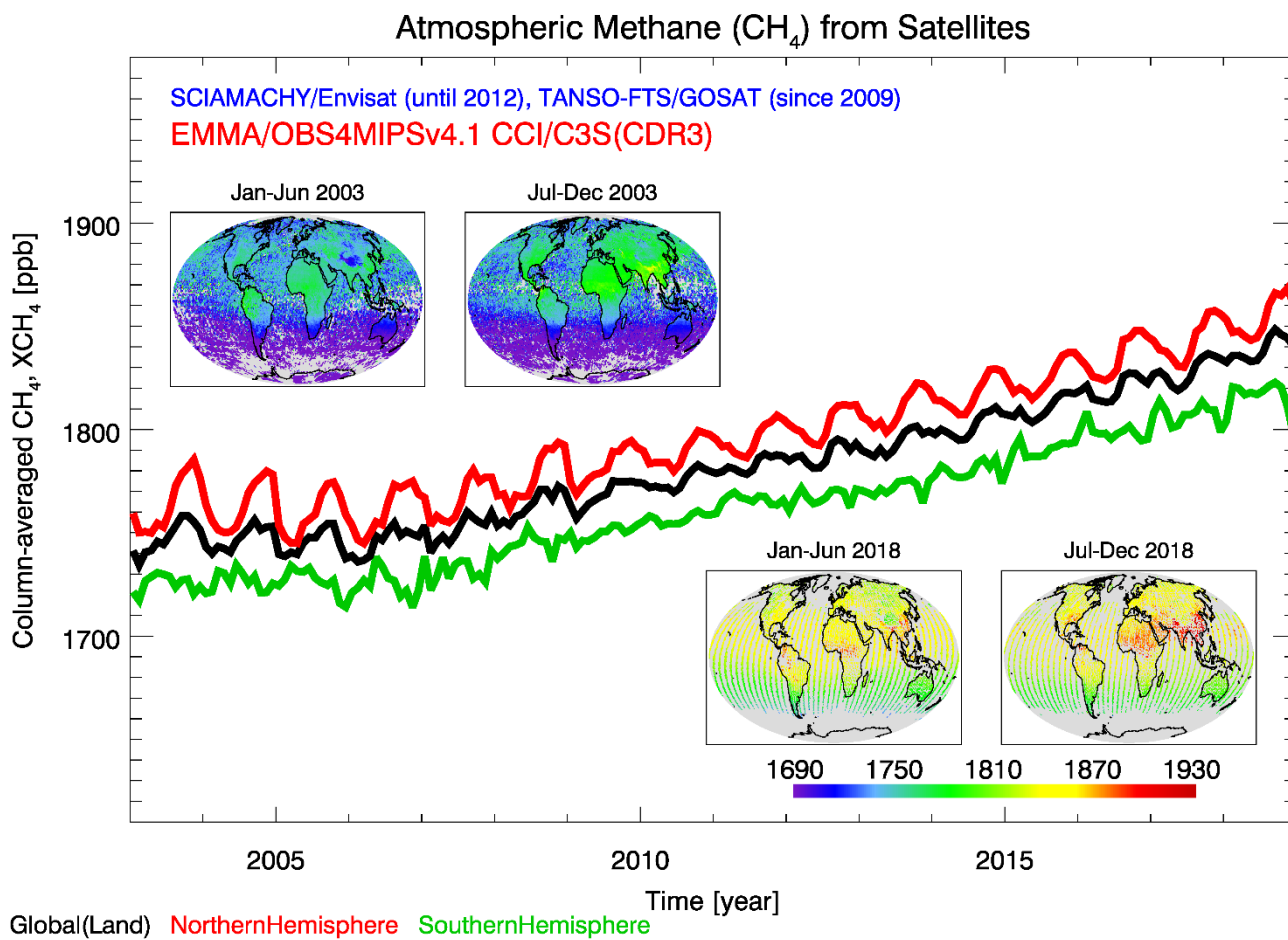
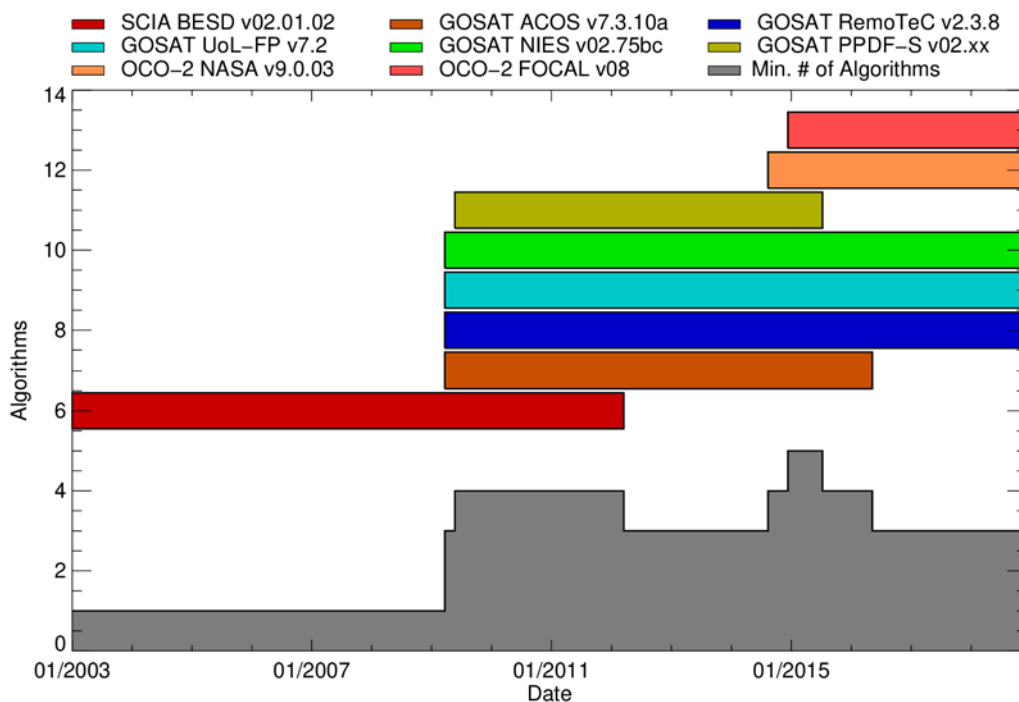


Figure 2: As Fig. 1 but for  $\text{XCH}_4$ .



950



**Figure 3: Individual satellite sensor XCO<sub>2</sub> data products contributing to the merged XCO<sub>2</sub> data products (see Tab. 1 for details). The required minimum number of contributing products is shown by the grey area.**

955

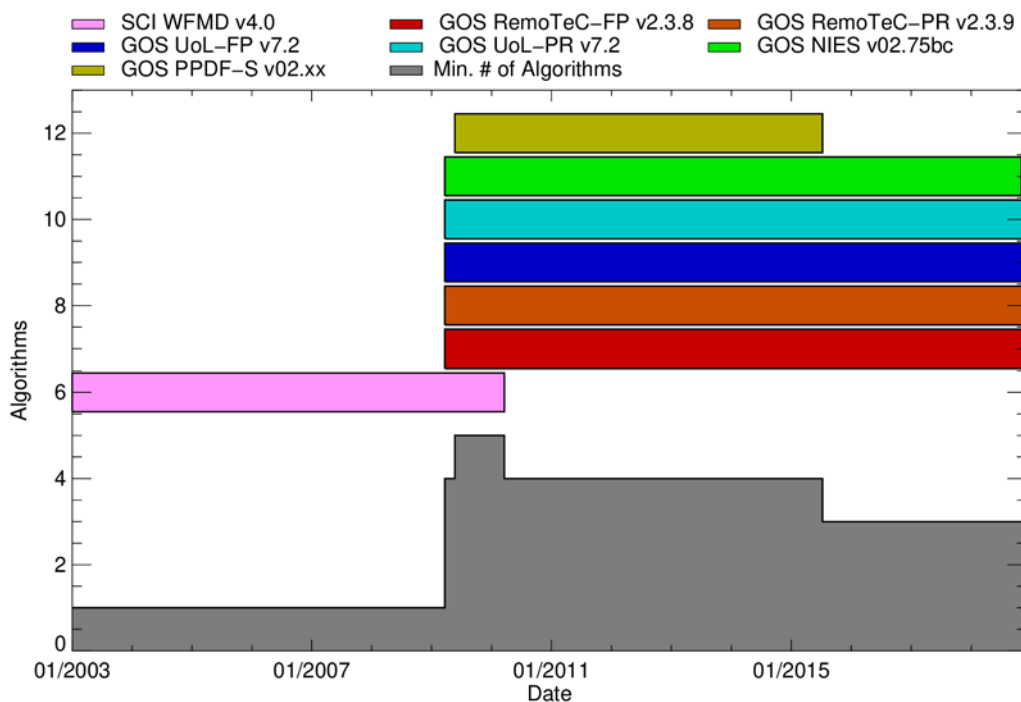
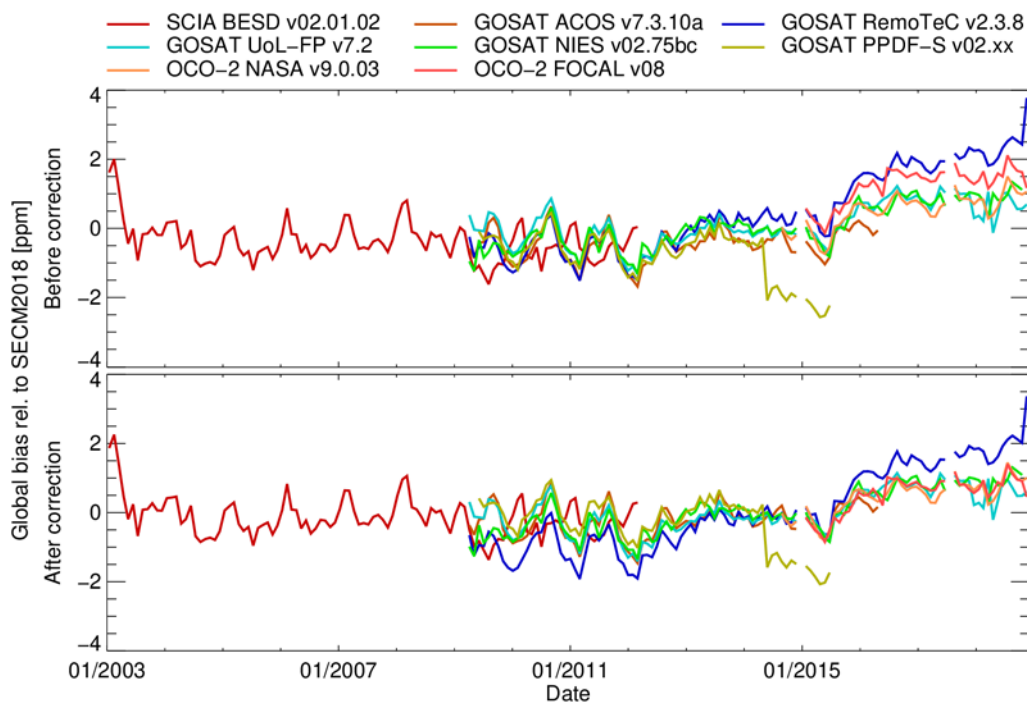
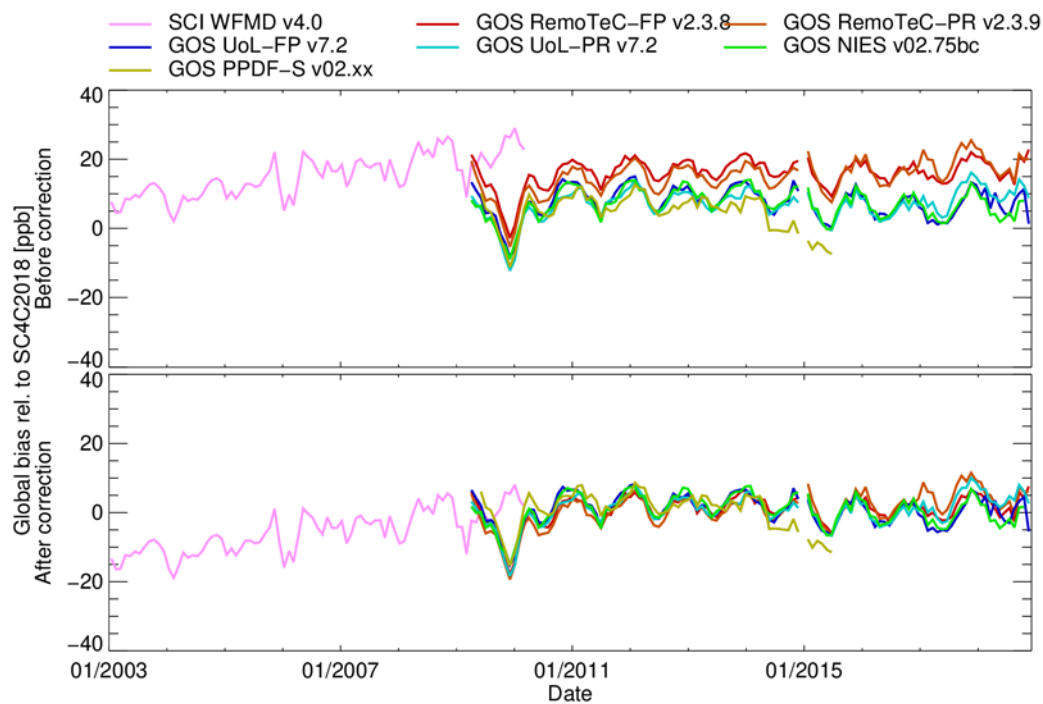


Figure 4: As Fig. 3 but XCH<sub>4</sub>. For details on each product see Tab. 2.



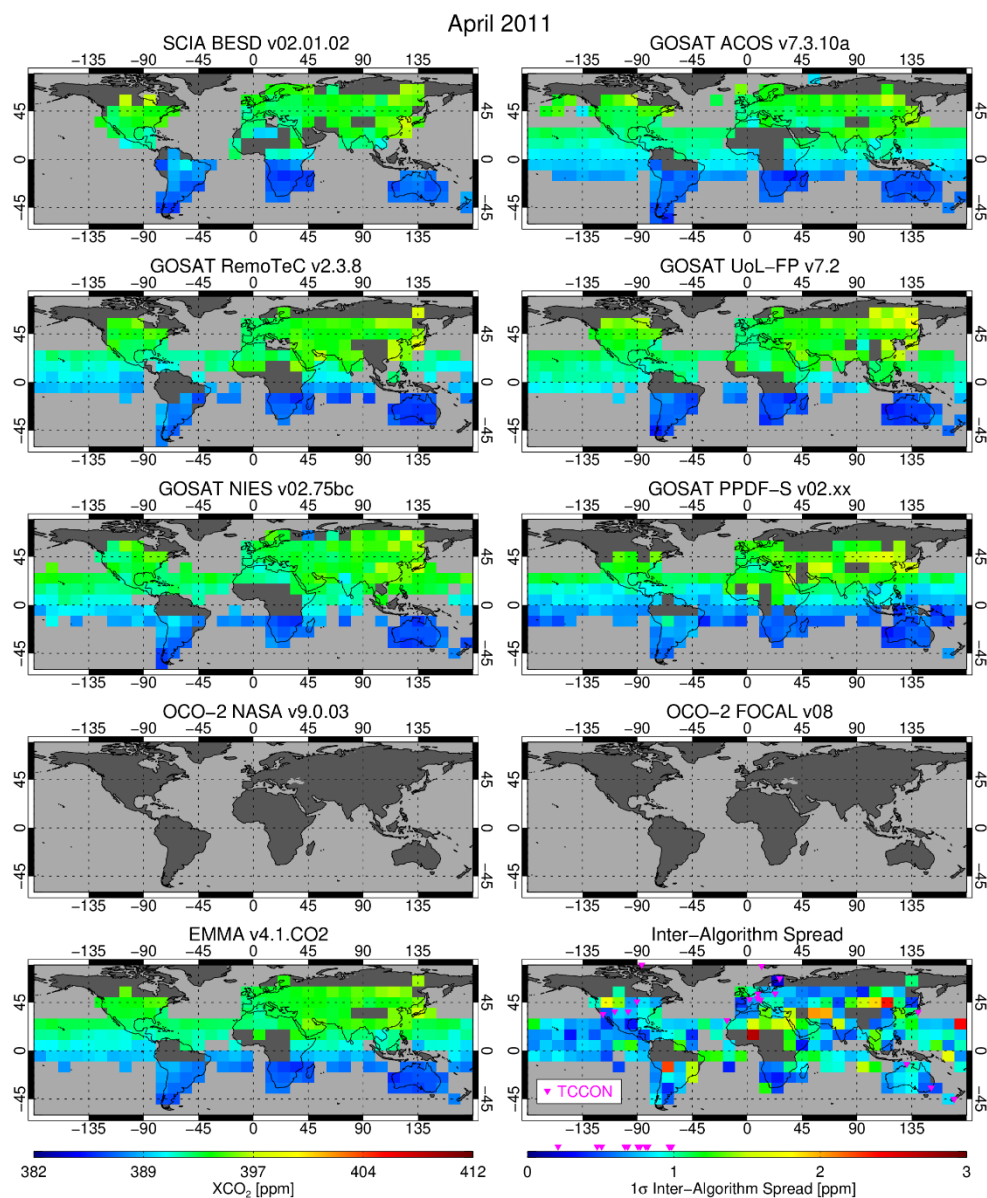
965 **Figure 5: Global bias correction as applied by EMMA to the individual satellite XCO<sub>2</sub> input data products. The top panel shows the difference relative to the SECM2018 model (computed as satellite - model) before the correction and the bottom panel shows the difference after correction.**



970

Figure 6: As Fig. 5 but for XCH<sub>4</sub> and using methane model SC4C2018.

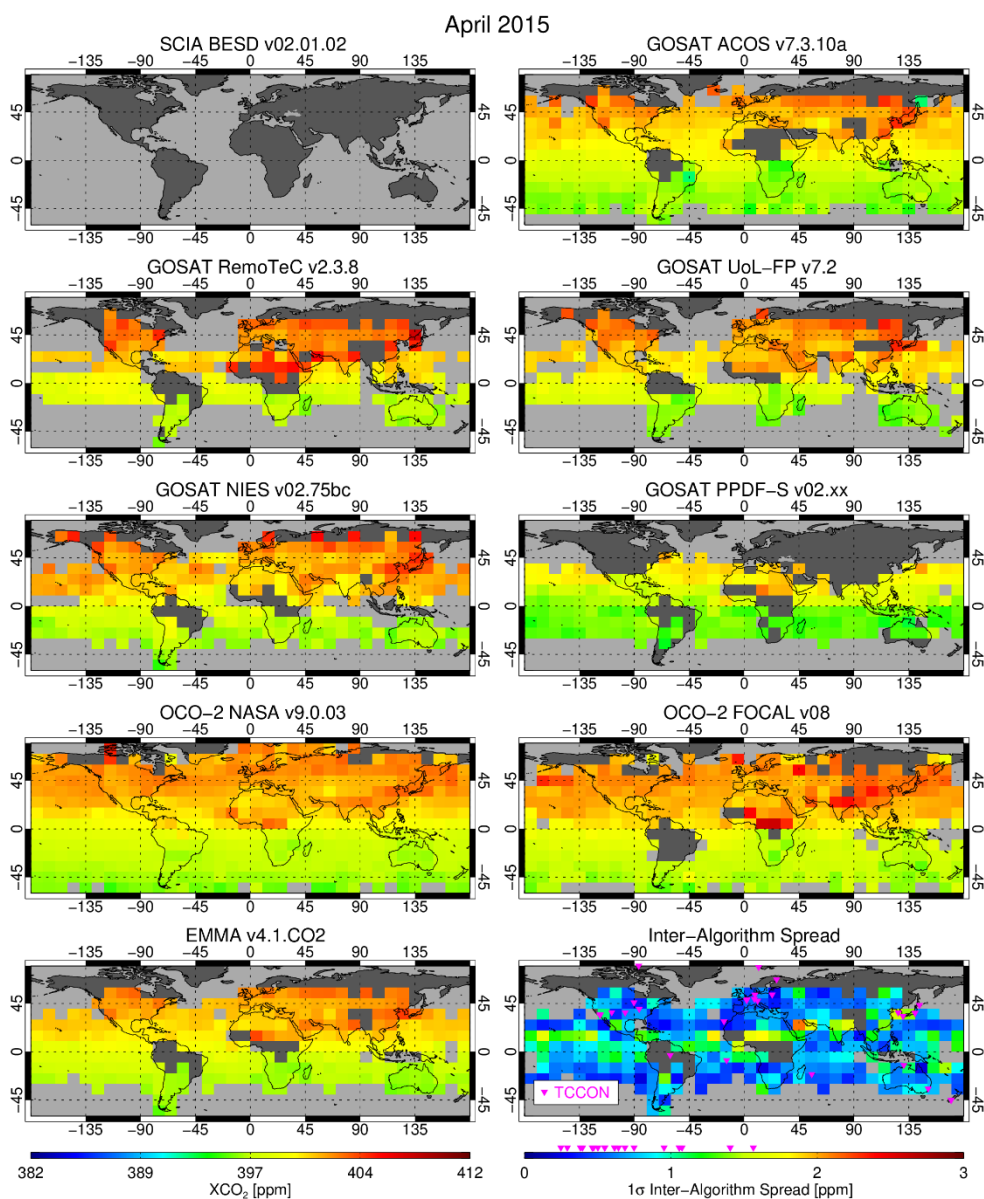




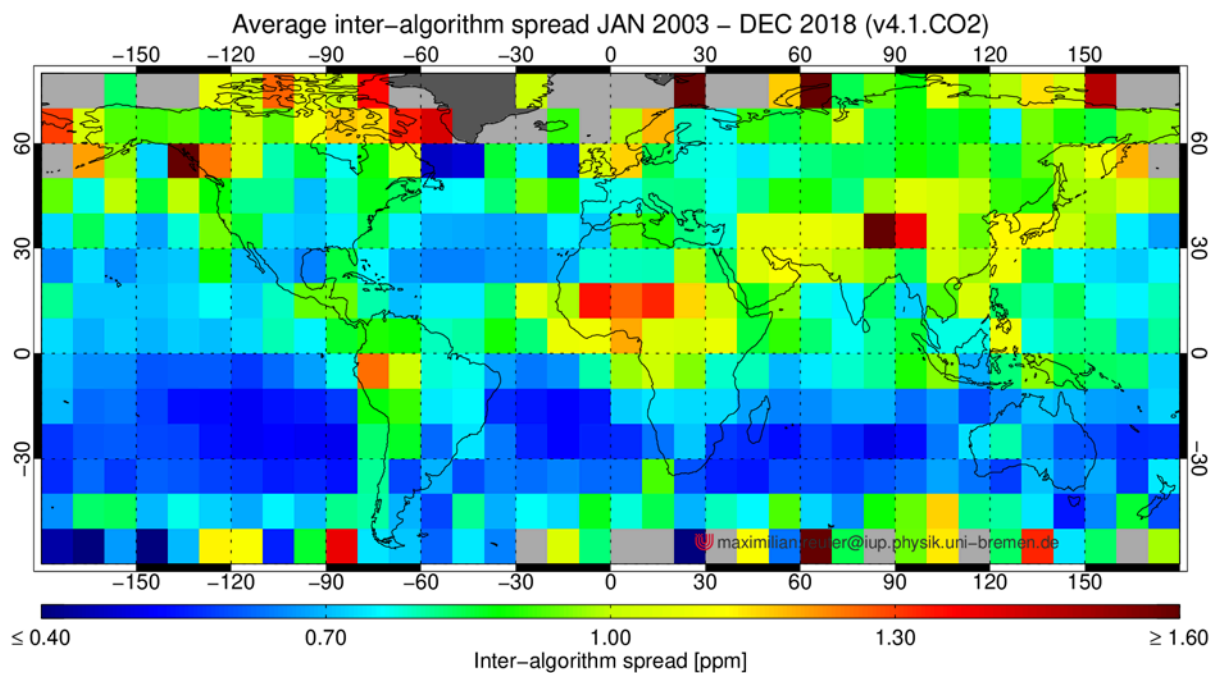
975

**Figure 7:** April 2011  $XCO_2$  at  $10^\circ \times 10^\circ$  spatial resolution showing (i) the individual sensor/algorithm input data sets (panels in rows 1-4; see Tab. 1 for details), and (ii) EMMA  $XCO_2$  (bottom left) and (iii) the Inter-Algorithm Spread (IAS, 1-sigma) as computed by EMMA (bottom right, see main text for details). Also shown in the bottom right panel are the locations of the TCCON sites (pink triangles) and the range of IAS values covered by them (see colour bar). Note that the OCO-2 maps (row 4) are empty because this satellite was launched after April 2011 (see Fig. 8 for OCO-2  $XCO_2$ ).

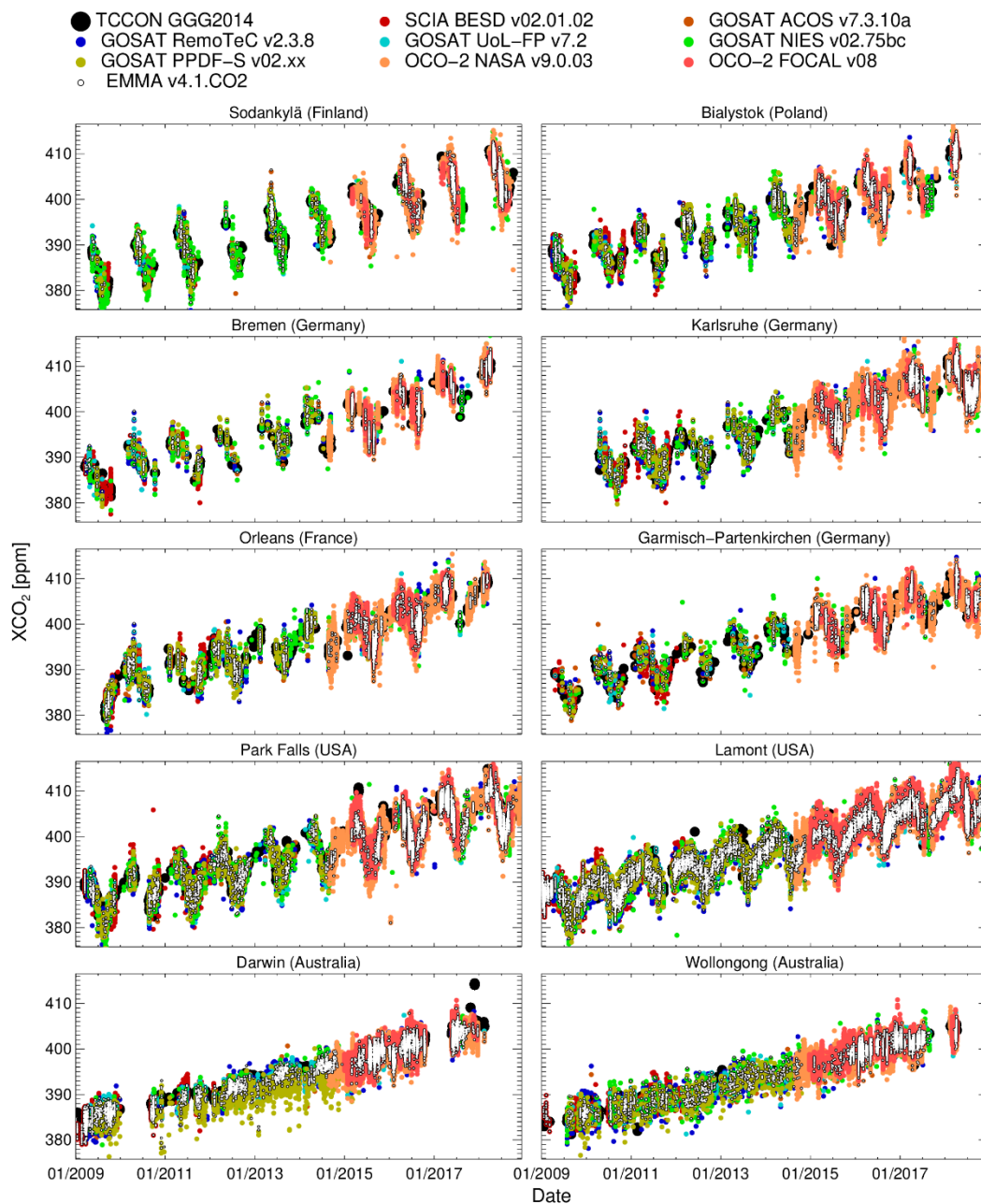
980



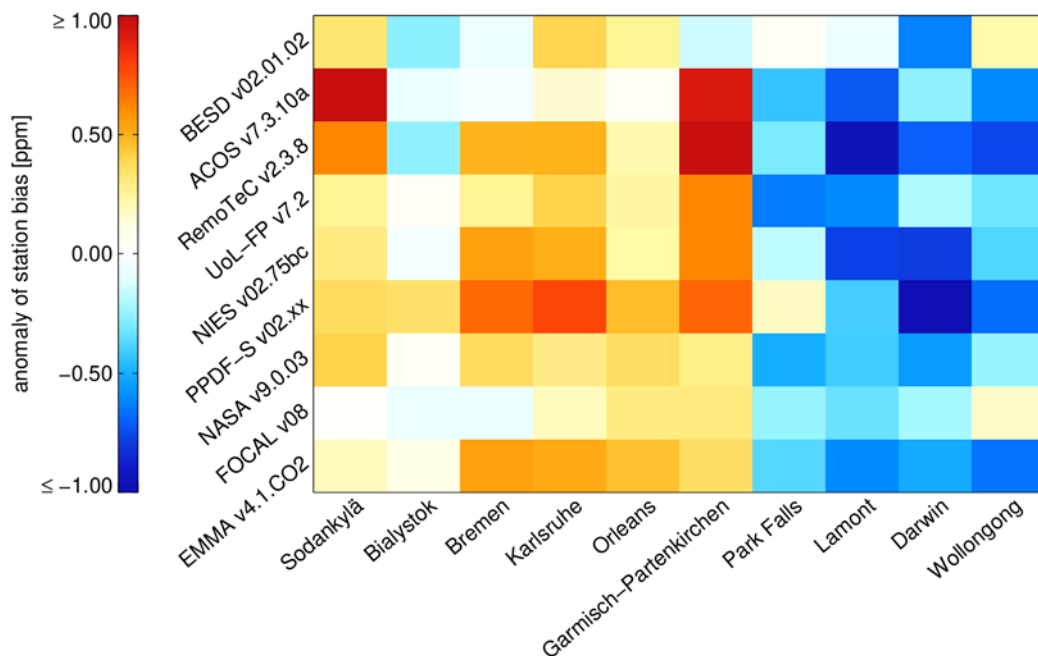
985 **Figure 8:** As Fig. 7 but for April 2015. Note that the SCIAMACHY/BESD map (top left) is empty because this product ended in April 2012 (see Fig. 7 for SCIAMACHY/BESD XCO<sub>2</sub>).



990 **Figure 9: Average XCO<sub>2</sub> inter-algorithm spread (1-sigma) during 2003-2018. As can be seen, the scatter is typically around 1 ppm except over parts of the tropics (in particular central Africa) and at high latitudes, where the scatter can be larger.**



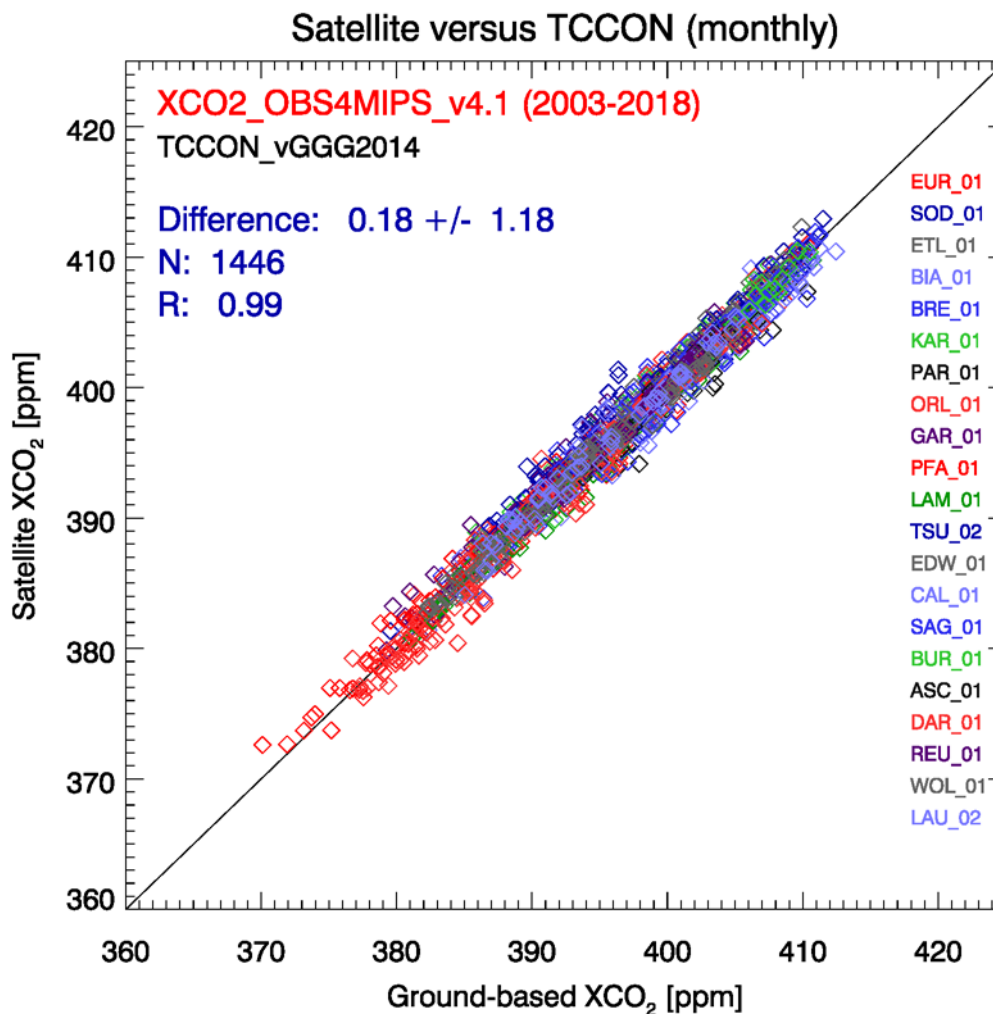
995 **Figure 10:** XCO<sub>2</sub> time series at 10 TCCON sites during 01/2009 – 12/2018 as obtained using the EMMA quality assessment method. TCCON GGG2014 XCO<sub>2</sub> is shown as thick black dots, the individual satellite L2 input products are shown as coloured dots and the EMMA product is shown as white circles with black borders. The derived numerical values are listed in Tab. 4.



1000

**Figure 11: Average XCO<sub>2</sub> differences (satellite – TCCON) for the different satellite XCO<sub>2</sub> products at 10 TCCON sites as used by the EMMA assessment method. The differences are shown as anomalies, i.e., the sum of the values corresponding to a given row is zero.**

1005



1010

Figure 12: Summary of the comparison of product XCO<sub>2</sub>\_OBS4MIPS with TCCON monthly mean XCO<sub>2</sub>. The comparison is based on 1446 monthly values. The mean difference (satellite - TCCON) is 0.18 ppm and the standard deviation of the difference is 1.18 ppm. The linear correlation coefficient R is 0.99.

1015



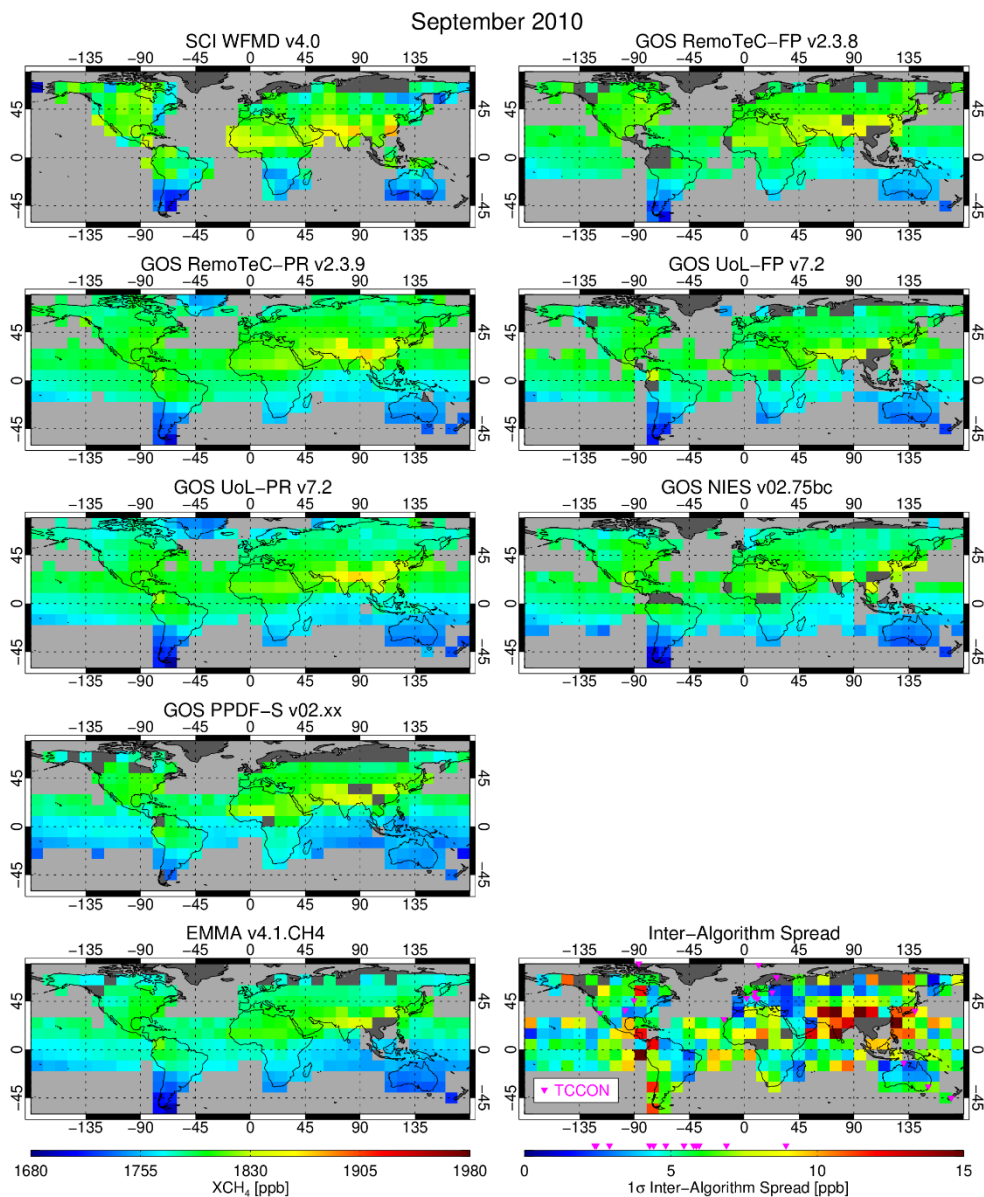
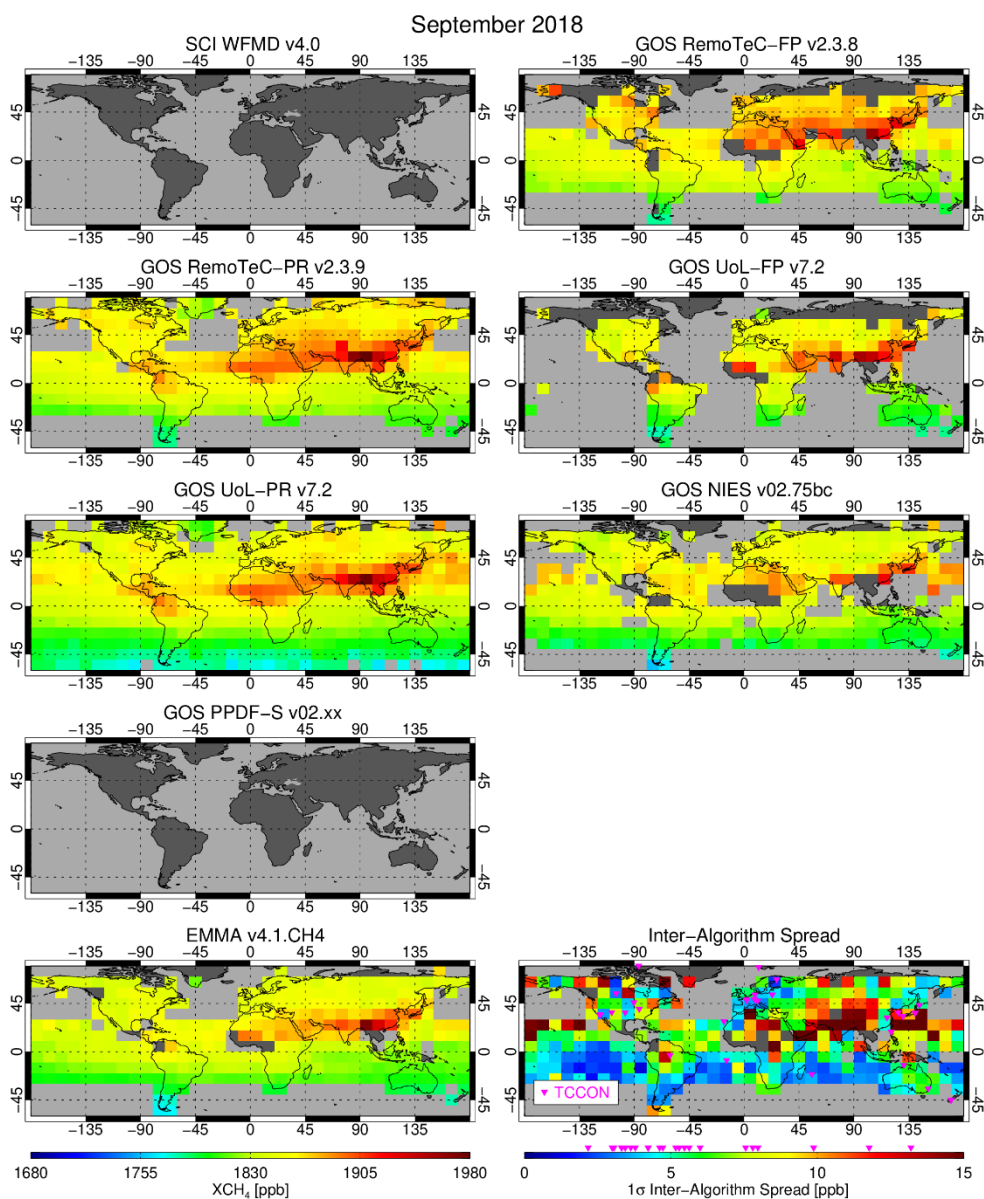
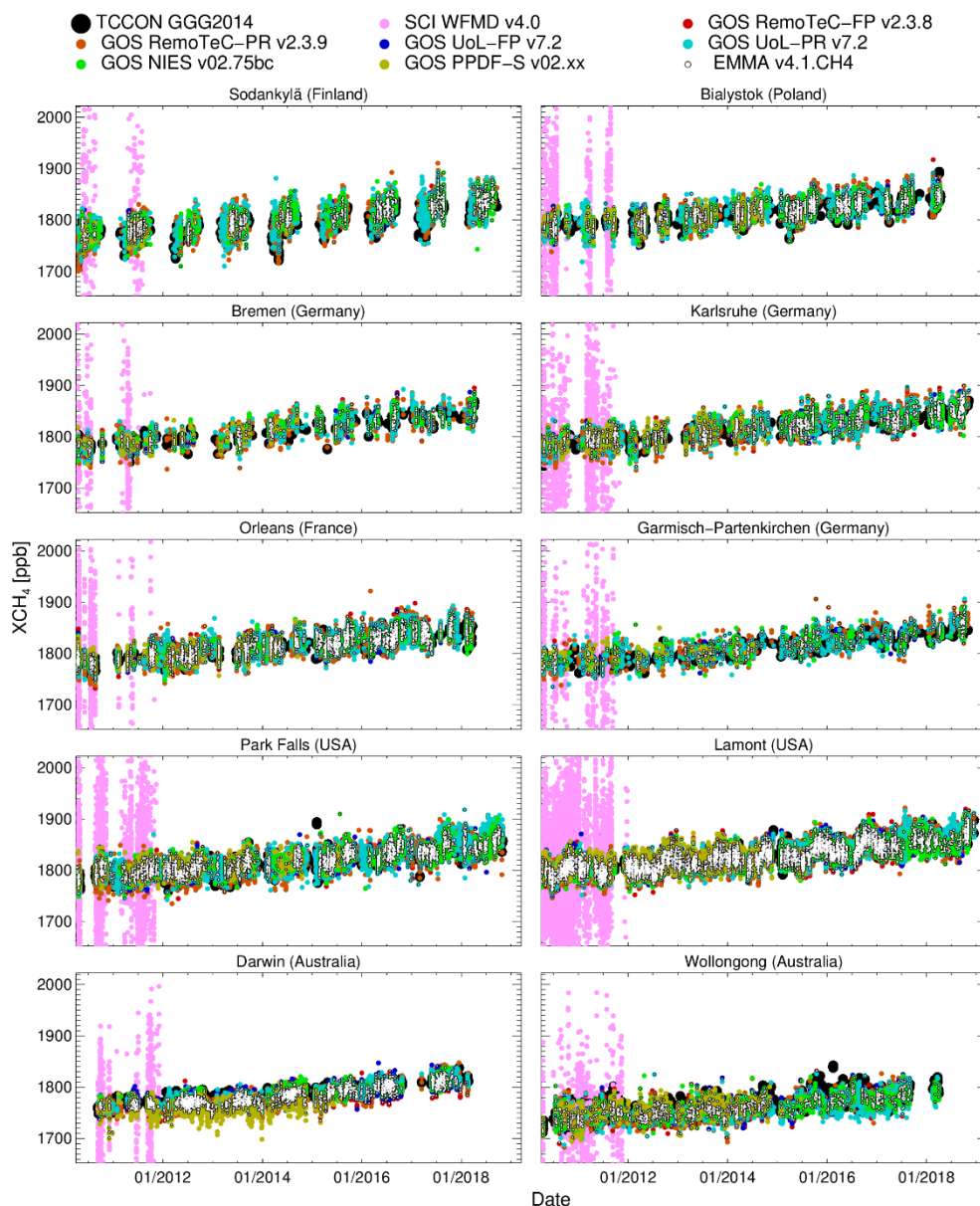


**Figure 13: September 2010 XCH<sub>4</sub> at 10°x10° spatial resolution showing (i) the individual sensor/algorithm input data sets (panels in rows 1-4; see Tab. 2 for details), (ii) EMMA XCH<sub>4</sub> (bottom left) and (iii) the Inter-Algorithm Spread (IAS, 1-sigma) as computed by EMMA (bottom right, see main text for details). Also shown in the bottom right panel are the locations of the TCCON sites (pink triangles) and the range of IAS values covered by them (see colour bar).**

1020



1025 **Figure 14:** As Fig. 13 but for September 2018. Note that the SCIAMACHY/WFMD map (top left) is empty because this product ended in April 2012 (see Fig. 13 for SCIAMACHY/WFMD XCH<sub>4</sub>). For product GOSAT/PPDF (row 4) no data were available for this month (see Fig. 13 for GOSAT/PPDF XCH<sub>4</sub>).



1030

**Figure 15: XCH<sub>4</sub> time series at 10 TCCON sites during 04/2010 – 12/2018 as obtained using the EMMA quality assessment method. TCCON GGG2014 XCH<sub>4</sub> is shown as thick black dots, the individual satellite L2 input products are shown as coloured dots and the EMMA product is shown as a white circles with black borders. The derived numerical values are listed in Tab. 7.**

1035

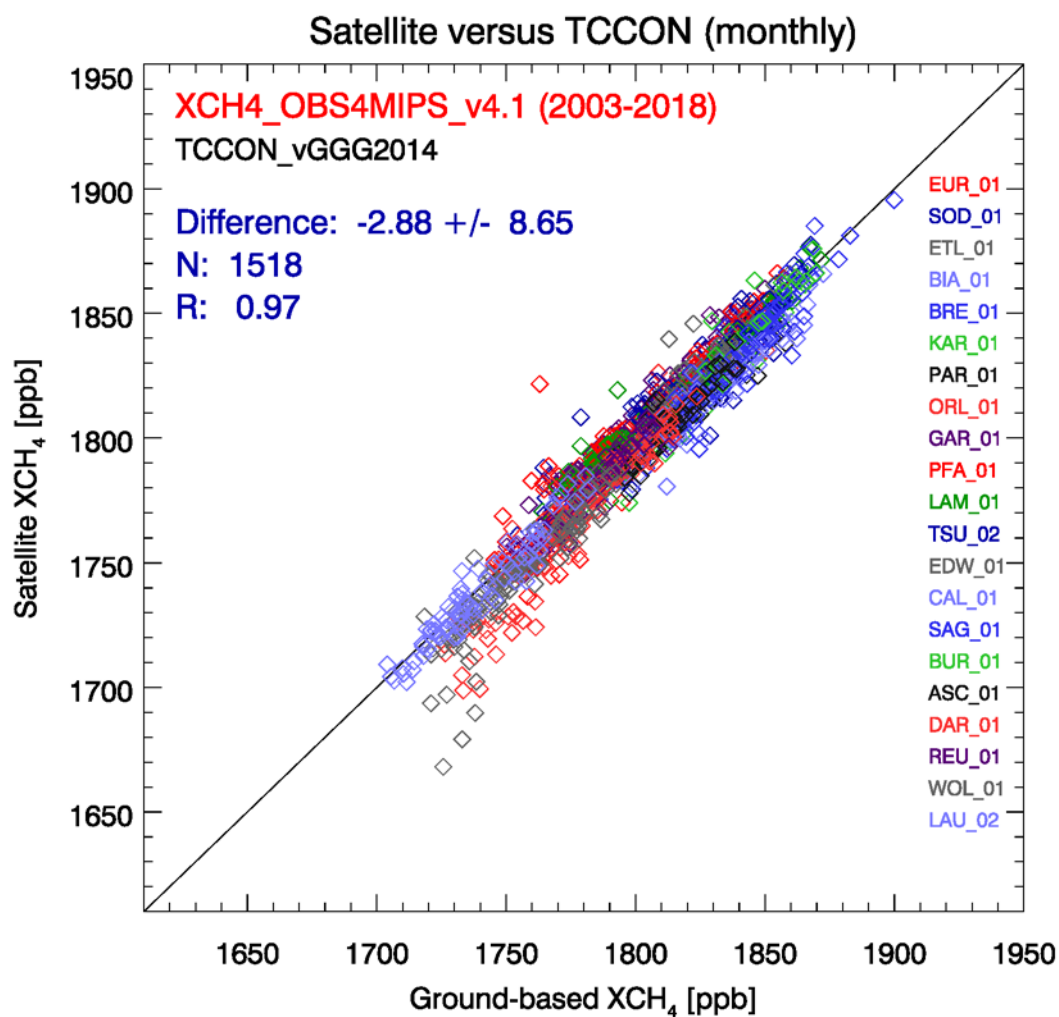
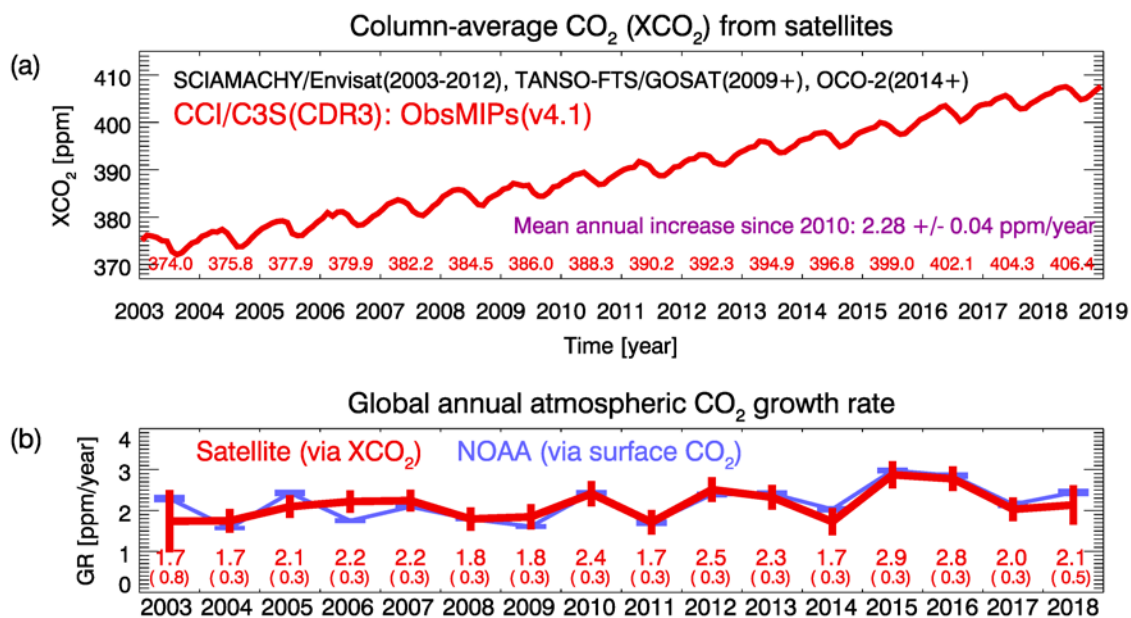


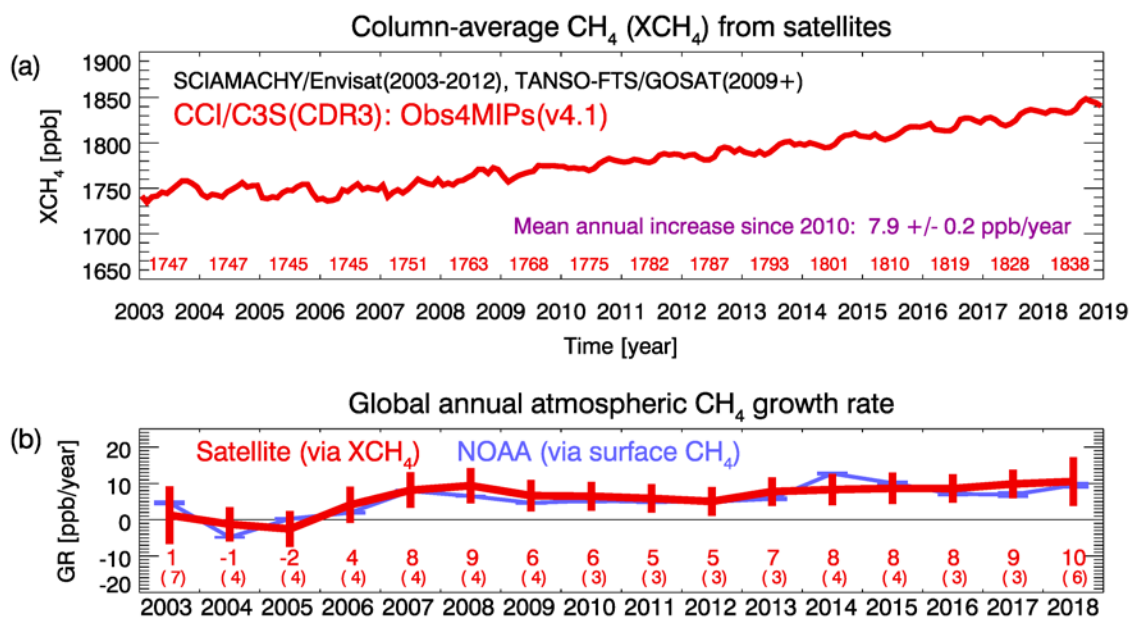
Figure 16: Summary of the comparison of product XCH4\_OBS4MIPS with TCCON monthly mean XCH4. The comparison is based on 1518 monthly values. The mean difference (satellite - TCCON) is -2.88 ppb and the standard deviation of the difference is 8.65 ppb. The linear correlation coefficient R is 0.97.



1045

**Figure 17:** (a) Monthly values of the globally averaged XCO<sub>2</sub> (over land) as computed from the OBS4MIPS version 4.1 XCO<sub>2</sub> data product. The corresponding annual mean XCO<sub>2</sub> values are also listed. The increase during 2010-2018 is 2.28 ± 0.04 ppm/year as obtained via a linear fit. (b) Annual XCO<sub>2</sub> growth rates (red, with 1-sigma uncertainties; the corresponding numerical values are also listed with 1-sigma uncertainty in brackets) and CO<sub>2</sub> growth rates from NOAA (shown in blue) obtained from marine surface CO<sub>2</sub> observations.

1050



1055 **Figure 18:** (a) Monthly values of the globally averaged XCH<sub>4</sub> (over land) as computed from the OBS4MIPs version 4.1 XCH<sub>4</sub> data product. The corresponding annual mean XCH<sub>4</sub> values are also listed. The increase during 2010-2018 is 7.9 ± 0.2 ppb/year as obtained via a linear fit. (b) Annual XCH<sub>4</sub> growth rates (red, with 1-sigma uncertainties; the corresponding numerical values are also listed with 1-sigma uncertainty in brackets) and CH<sub>4</sub> growth rates from NOAA (shown in blue) obtained from marine surface CH<sub>4</sub> observations.

1060

1065